FACTORS CONTROLLING DIFFUSIVE CO_2 PRODUCTION AND TRANSPORT IN THE CEDARBURG BOG, SAUKVILLE, WISCONSIN

by

Emily K. Joynt

A Thesis Submitted in

Partial Fulfillment of the

Requirements for the Degree of

Master of Science

in Geosciences

at

The University of Wisconsin-Milwaukee

May 2017

ABSTRACT

FACTORS CONTROLLING DIFFUSIVE CO_2 PRODUCTION AND TRANSPORT IN THE CEDARBURG BOG, SAUKVILLE, WISCONSIN

by

Emily K. Joynt

The University of Wisconsin-Milwaukee, 2017
Under the Supervision of Professor Timothy Grundl

Wetlands are vital components of the carbon cycle, containing an estimated 20-30% of the global soil carbon reservoir. The Cedarburg Bog of southeastern Wisconsin boasts a myriad of wetland habitats including the southernmost string bog found in North America. Soil carbon dioxide (CO_2) behavior in these systems is the response of multiple interdependent variables that are, collectively, not well understood. Many studies have measured and modeled soil CO_2 flux (soil respiration) based on isolated, intermittent measurements that do not account for the full range of soil CO_2 flux intensity. In the Cedarburg Bog, high-resolution measurements of soil CO_2 flux were recorded over two field seasons using a LI-COR 8100A soil gas flux analyzer at 30 minute (May-Nov., 2014) and 60 minute (June-Oct., 2015) intervals. Additionally, soil moisture and temperature data were collected, and weather station variables (atmospheric temperature, radiation, wind, pressure, precipitation) were acquired for correlations. Stable isotope signatures were interpreted from a peat core ($\delta^{13}C$, $\delta^{15}N$) and from gaseous CO_2 at the surface ($\delta^{13}C$) to determine sources of soil respired CO_2.

The intensity of soil CO_2 flux was broadly distributed across the entire data set, ranging from less than 1 to over 650 mg/min-m^2. Average for all soil CO_2 flux measured was 6.49 mg/min-m^2, with a median of 3.39 mg/min-m^2. Soil respiration was attributed to two main

sources: 1) microbial respiration, and 2) root respiration (including rhizo-microbial respiration). Microbial respiration was, in part, influenced by soil temperature, and produced a constant, low flux (< 5 mg/min-m^2). The addition of root respiration generally resulted in a diurnal increase in soil CO_2 flux (medium flux, 5-50 mg/min-m^2) in response to radiation and temperature trends reflecting photosynthetic assimilation of CO_2. In addition, infrequent, high flux (> 50 mg/min-m^2) were observed, but were not correlated to the included parameters. Although high flux occurred much less frequently, it produced a significant amount of the CO_2 mass respired from the soil. Correlations between soil CO_2 flux and controlling parameters were addressed using JMP; multiple linear regression models presented weak and significant correlations due to the absence of lag/response time variables for assimilation and transport mechanisms of CO_2. Wetland soils are structurally complex, and can be highly variable through time; improving correlations for soil respiration models requires high-resolution data sets, and determination of lag/response times of CO_2 transport processes above ground and in the soil.

TABLE OF CONTENTS

LIST OF FIGURES

ACKNOWLEDGMENTS

This project was made possible with support from so many different people in so many different ways. I would first like to express my deepest and sincerest gratitude to Timothy Grundl and Weon Shik Han for their patience and support as advisors. Their energy and encouragement has influenced me beyond the reaches of this project, and will stay with me long into the future. Thank you to my committee members, Erik Gulbranson and Shangping Xu, for their constructive criticism, and an additional thanks to Erik for his guidance in conducting isotope analyses in the field and in the laboratory.

Much appreciation goes to James Reinartz and Gretchen Meyer of the UW-Milwaukee Field Station for their cooperation in collecting and sharing field data in the Cedarburg Bog. I would also like to thank the many individuals who helped collect and process this field data: Jack Graham, Ethan Guyant, Kyungdoe Han, Na-Hyun Jung, Cassandra Wolf, John Teppler, Laura Fields-Sommers, Kate Pauls, Megan Barlow, and Harris Byers. I cannot thank you each enough for your efforts.

An enormous debt of gratitude is owed to the UW-Milwaukee Geosciences Department. Over the last 6 years, as an undergraduate and then graduate student in this department, I have been fortunate to know and learn from so many inspiring people. It was here that I, quite unexpectedly, found my passion in Geology; every one of you has played a part in shaping my growth as a person and a scientist, and for that I am indescribably grateful.

Finally, I would like to thank my family. To my parents, Karen, Gordon, and Rick, whose generosity inspires me every day of my life; and to my brothers, Barry, Michael, and Andrew, for always looking out for their little sister. I would not be where I stand today without each of you.

1. Introduction

Wetlands serve a multitude of vital roles across the Earth; habitats for biodiversity including rare and endangered plant and animal species, natural pollutant filtration systems, flood relief, peat harvesting, and priceless aesthetic and cultural values (Brooker et al. 2014; Mitsch et al. 2015). Although wetlands cover only an estimated 5-8% of the Earth's terrestrial surface, wetlands store approximately 20-30% of global soil carbon (Mitsch et al. 2015). Natural cycling of nutrients in wetlands results in either the absorption or emission of greenhouse gases such as methane (CH_4), nitrous oxide (NO_2), and carbon dioxide (CO_2). The rate at which wetlands decompose, and their potential to emit greenhouse gases, is dependent on multiple biological and physical factors, and processes above and below the surface (IPCC 2013).

Wetlands are recognized in many studies for the uncertainty in soil carbon storage potential, especially under changing climatic conditions (Comas et al. 2014; Darenova et al. 2016; Dinsmore et al. 2013; Hashimoto and Komatsu 2005; Liu et al. 2015; Rosenberry et al. 2006). On a global scale, wetlands are estimated to sequester 1,000 Tg (10^{15} g) of carbon per year from the atmosphere (Mitsch et al. 2015). How wetlands adapt and respond to changing climate and land use conditions depends, in part, on what controls the production and transport of greenhouse gases such as CO_2.

The largest emission source of CO_2 in terrestrial ecosystems is soil CO_2 flux, also known as soil respiration (Goffin et al. 2014). Soil respiration represents one component of net ecosystem exchange (NEE), the positive or negative balance of CO_2 in an ecosystem relative to the atmosphere. NEE studies identify environments as net sources or net sinks of CO_2 based on an overall balance between CO_2 uptake (photosynthetic assimilation) and release (soil respiration

and above ground respiration). Wetlands are commonplace in this type of research based on carbon storage potential, and the concern for increased CO_2 emissions under changing climate conditions. Studies on soil CO_2 flux focus specifically on the soil respiration component of NEE, using soil gas monitoring chambers to directly measure the rate of CO_2 moving from the soil to the surface.

The desire to quantify wetland emissions has led to an abundance of research focusing on soil CO_2 flux. Much of this research, however, relies on data sets of limited temporal and spatial measurement resolution. Studies overwhelmingly collect and represent soil CO_2 flux data based on isolated, intermittent measurements. Measurements are integrated over an expansive amount of time, threatening to grossly over- or underestimate soil respiration and subsequently create models that largely simplify trends and controls. (Görres et al. 2016)

Soil CO_2 production and transport varies in response to numerous criterion. Soil CO_2 production stems from multiple sources (i.e. microbial activity, root respiration) and subsequent transport to the surface is dependent on physical properties of soil media. To improve predictions of wetland response to climate and land use changes, a more detailed representation of these relationships must be developed. This study provides an unparalleled high-resolution, long-term temporal data set of soil CO_2 flux (soil respiration) in a temperate wetland alongside controlling biological and physical parameters.

2. Research Site

The Cedarburg Bog is a Wisconsin State Natural Area, a National Natural Landmark, and one of the largest wetlands in southern Wisconsin (Grittinger, 1971). During the Wisconsinian glaciation, circa 12 ka, the Laurentide Ice Sheet terminated along the eastern boundary of the

current Cedarburg Bog, forming a pro-glacial lake lined with clay. Subsequent deposition of plant and animal material along the clay-lined lake bottom created a sediment layer that exists within roughly 1-3 meters of the modern peat surface (Reinartz 1985). Continued accumulation of peat and muck under favorable climate and hydrological conditions has established the habitats observed today (Figure 1a) (Graham, 2015).

Wetland classification is generally based on the hydrologic and biologic characteristics of an environment. In terms of hydrology, a precipitation fed wetland is classified as a 'bog', and a groundwater fed wetland is classified as a 'fen'. The Cedarburg Bog is an area of groundwater recharge; the dissolution of Silurian dolomite bedrock in groundwater maintains the near neutral pH of surface water. Based on hydrology, the Cedarburg *Bog* therefore classifies as a fen (Kline 1991). Biologically speaking, however, the Cedarburg Bog supports many plant species typically found in bogs such as *Sphagnum* moss (Reinartz 1985; Mitsch and Gosselink 2015). The unique diversity of the Cedarburg Bog makes it elusive to any individual wetland classification.

At the heart of the Cedarburg Bog lies the southernmost string bog (also known as a 'patterned peatland' or 'Strangmoor') identified in North America. The string bog is one of seven different wetlands classified in the area of the Cedarburg Bog, and supports plant and animal species typically found much further north. The morphology consists of raised hummocks (strings) of stunted cedar and tamarack trees alternating sedge-dominated hollows (flarks) that form perpendicular to the direction of water flow. In the Cedarburg Bog, the 'string' ridges range between < 0.1 m to > 0.3 m higher than the inter-fingered flark mats. Strings are up to 6 m wide, and in some cases run more than 30 m before terminating or adjoining another string (Grittinger 1971). These patterns are thought to form from the linear expansion of initial downslope pools

compounded with peat accumulation in adjacent strings (Mitsch et al., 2015). The surrounding area is composed of various emerging aquatic wetlands, sedge meadow, shrub carr, an upland hardwood forest (glacial islands), and several interspersed lakes. (Reinartz 1985)

The expansive 2,200-acre natural area is home to hundreds of different plant species and serves as breeding and migratory grounds for many different bird species (Reinartz, 1985). The University of Wisconsin-Milwaukee Field Station maintains facilities on over 300 acres outside the western entrance to the Cedarburg Bog, and has constructed a series of trails and floating boardwalks that end in the string bog (Figure 1b). The management of this area provides a rare opportunity to access a well preserved, complex, diverse, and isolated wetland environment, and as such is an ideal candidate for this study.

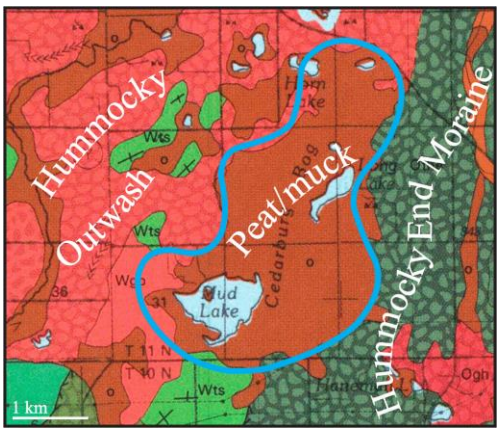

(a)

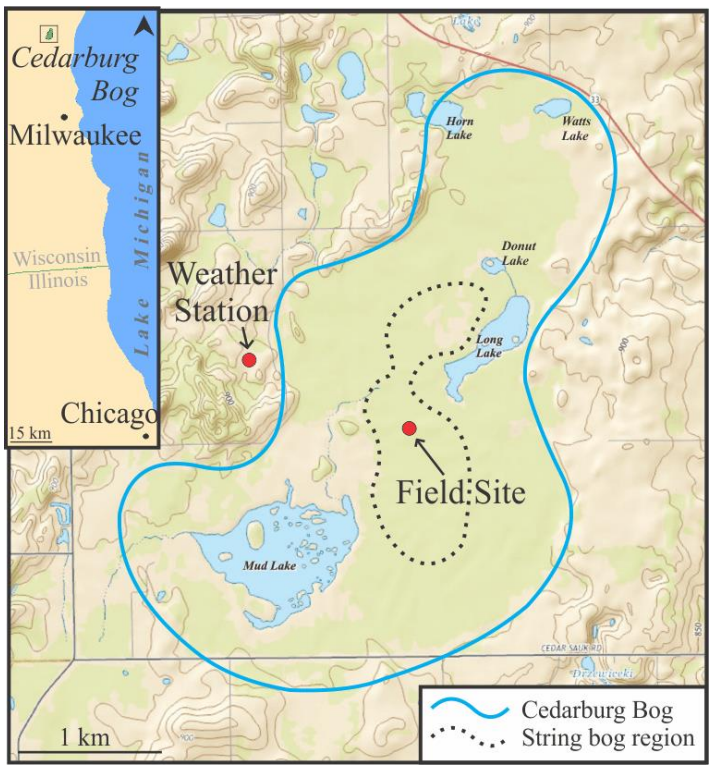

(b)

Figure 1: (a) Quaternary geology of the Cedarburg Bog and surrounding region (modified from Wisconsin Geological & Natural History Survey). (b) Area map of the Cedarburg Bog and string bog region, each outlined. Field site and weather station locations marked (modified from Wisconsin Department of Natural Resources).

3. Materials and Methods

Data collection was sourced from multiple field and laboratory instruments over two separate field seasons, 2014 and 2015. With the exception of weather data, all measurements were collected within the centrally located string bog region of the Cedarburg Bog (Figure 1b). A series of trails and floating boardwalks grant access to this area from the western boundary of the Cedarburg Bog, terminating at the designated "Field Site" location. Instruments were located along the perimeter of the boardwalk (Figure 2), and in the case of prolonged exposure, housed on a partially enclosed platform for protection from field conditions (i.e. high water table, high temperatures).

An automated soil gas flux system remained on the platform for the duration of each field season, measuring soil CO_2 concentration and flux (Figure 2, right-hand insert). Additional soil temperature and moisture content were measured with external probes. Periodically, a stable isotope analyzer was deployed adjacent to the platform, collecting in situ carbon isotope signatures and concentrations from gaseous CO_2 at the surface (Figure 2, center insert). In addition to gaseous isotope signatures, a peat core from the string bog region was extracted and analyzed in the laboratory for stable carbon and nitrogen isotopes within the soil using a mass spectrometer and elemental analyzer (Figure 2, left-hand insert). A monitoring well equipped with a pressure transducer also recorded groundwater level (Figure 2). Potential for the string bog region to support a mobile peat surface led to further observation of groundwater trends using trail cameras. Finally, weather data (atmospheric temperature, humidity, pressure, precipitation, radiation, wind speed) were obtained from the UW-Milwaukee Field Station, located 1.2 km from the Field Site location (Figure 1b).

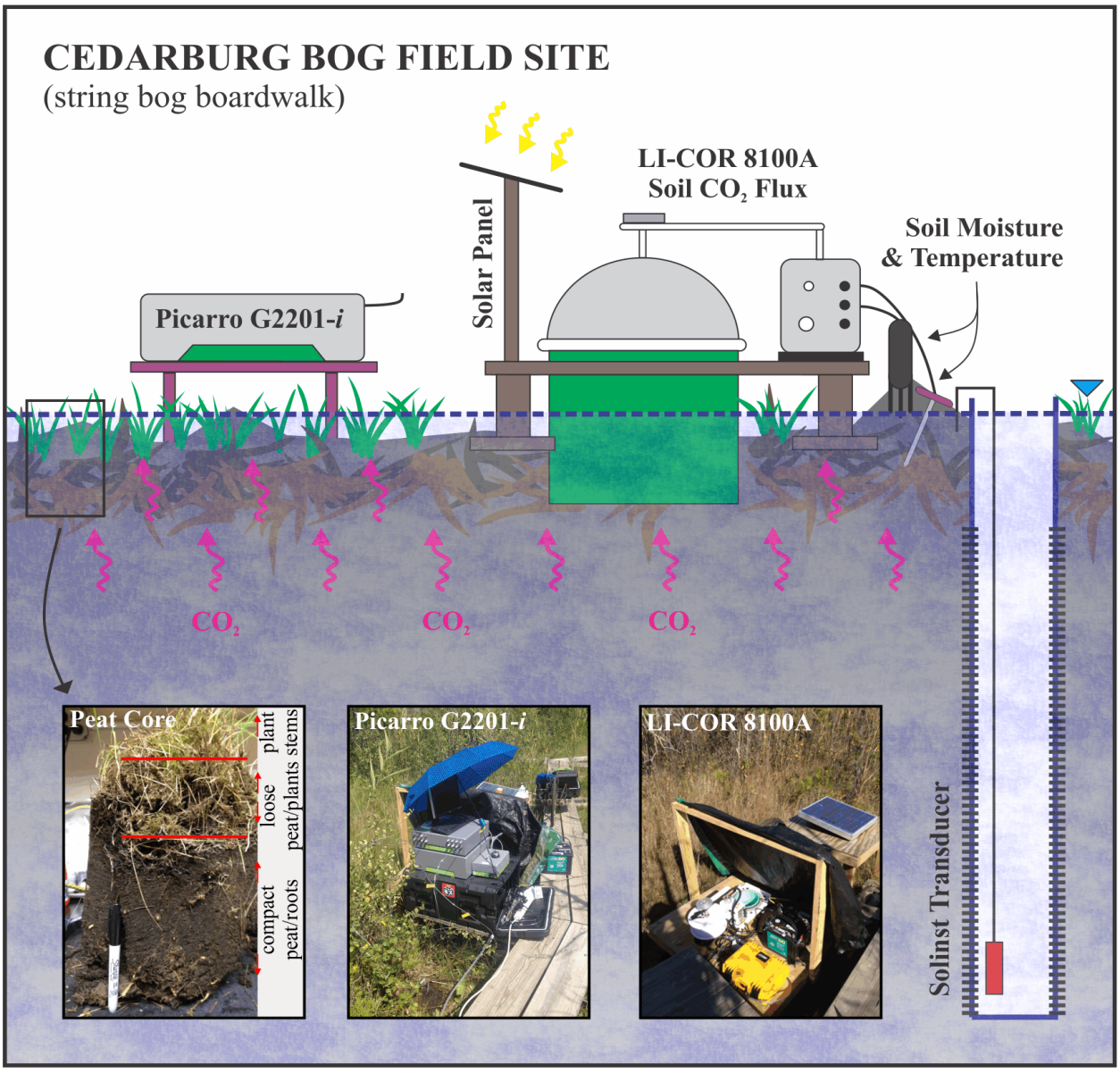

Figure 2: Conceptual field site model along boardwalk in the Cedarburg Bog. Photo inserts: peat core collected from string bog (left), Picarro stable isotope analyzer (center), and LI-COR soil gas flux analyzer (right) (image modified from Weon Shik Han 2015).

3.1 LI-COR 8100A Soil Gas Flux System

The LI-COR 8100A automated soil gas flux system was used to record soil CO_2 concentration and flux, and soil temperature and moisture, deployed as a long-term measurement chamber and given supplemental external power by two paralleled 12V deep cycle batteries connected to the Auxiliary Sensor Interface. Chamber measurements enclosed 4 vertically

stacked PVC collars (diameter = 20 cm) pushed into the compact peat to a depth of 5.72 cm in 2014, and 1.62 cm in 2015. Following each installment, plant material was removed from the chamber soil area. Although this instrument is designed to withstand a wide range of weather conditions, to ensure longevity the chamber and interface were housed on a raised wooden platform and covered on ¾ sides with a tarp (open due north). An accessory temperature probe was inserted to a depth of 25 cm beneath (2014) and beside (2015) the platform, collecting soil temperature in sync with CO_2 concentration and CO_2 flux data.

LI-COR data were collected over 90-second measurement periods with a 30-second dead band during both field seasons. The dead band period represents the time allowed for steady mixing after the chamber is closed; flux calculations disregard data collected during these initial mixing conditions. The first field season of this study (2014) was executed by multiple individuals, reflecting some inconsistency in measurement criteria (i.e. soil area, chamber offset). Using LI-COR's SoilFluxPro processing software, data sets were recalculated to reflect the appropriate parameters during measurement. Pre-purge represents the time allowed between measurements for chamber air to return to ambient air conditions. Post-purge represents the time following measurement, when the chamber begins to open, during which air continues to flow through the chamber. Pre- and post-purge values do not remain consistent across all data periods, but cannot be secondarily adjusted. All data sets have a post-purge time of 45 s, with the exception of the first period in 2014 (5/22-6/9/14) where a post-purge of 15 s was applied. Pre-purge values are either 15 or 30 s, but are not relevant for the majority of data periods since collection intervals allowed adequate time for the chamber area to return to ambient conditions between measurements (typically 30-60 min.). The only exception being the period of 7/9-7/10/14 where a 3 minute measurement interval was applied, leaving a much shorter period of

time in which the chamber could return to ambient conditions (30 s pre-purge followed by a 90 s measurement period).

In 2014, measurement intervals of 20-30 minutes allowed for continuous data records generally consisting of 4-5 days between late May and early November (Figure 3). For one 22-hour overnight period (July 9-10, 2014), measurements were collected every 3 minutes in order to enhance diurnal observations. Discontinuities between measurement periods in 2014 are variable and range from just a few hours to several weeks. In 2015, measurements were expanded to 60-minute intervals with added power from two solar panels directly charging the external 12V batteries. Under these conditions, continuous data records generally spanned periods of one to several weeks with measurement gaps typically less than one day, but no more than three days, between June and mid-October. In 2015, an accessory soil moisture probe was also placed in the peat beside the LI-COR platform, collecting measurements in sync with CO_2 concentration, CO_2 flux, and soil temperature.

To determine CO_2 concentration the LI-COR 8100A uses a closed chamber method measuring the rate of infrared photon absorption due to the presence of CO_2. Based on the rate of absorption inside the closed chamber, CO_2 concentration is measured over a designated length of time (observation length, 90 s), and CO_2 flux is in turn modeled from a series of exponential or linear regressions. Initial CO_2 concentration values are neglected from CO_2 flux calculations during a designated length of time (dead band, 30 s) for the closed chamber to establish mixing. These initial values are instead used in a separate regression of the first 10 seconds of measurements, the intercept of which represents conditions at the soil surface prior to chamber closure. In addition to CO_2 concentration, the LI-COR 8100A measures and records chamber

pressure, temperature, relative humidity, and water vapor concentration. Soil CO_2 flux (F_c, µmol/m^2s) is derived using these variables in the following equation:

$$F_c = \frac{10VP_0(1 - \frac{W_0}{1000})}{RS(T_0 + 273.15)} \frac{\partial C'}{\partial t}$$

where V is the chamber volume (cm^3), P_0 is the initial pressure (kPa), W_0 is the initial water vapor mole fraction (mmol/mol), R is the universal gas constant (8.314 m^3Pa/Kmol), S is the soil surface area (317.8 cm^2), T_0 is the initial air temperature (ºC), and $\partial C'/\partial t$ is the initial rate of change in water-corrected CO_2 mole fraction (µmol/mol) following the dead band period. (LI-COR, 2010)

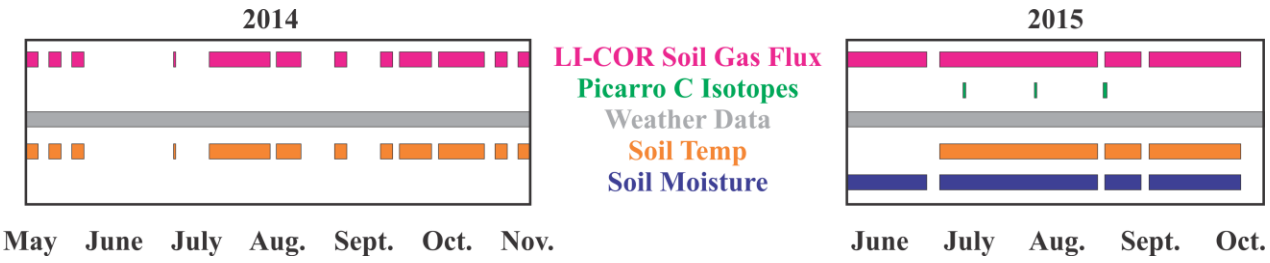

Figure 3: Measurement timeline of equipment used in the Cedarburg Bog during 2014 and 2015 field seasons.

Soil temperature measurements were collected using a Rugged Penetration Omega Thermocouple T-Handle 25 cm probe connected to the LI-COR Auxiliary Sensor Interface. Measurement intervals for both field seasons were collected in sync with chamber CO_2 flux data, with 2015 measurements beginning in early July. In 2014, the probe was placed directly beneath the LI-COR platform, but in 2015 was shifted to ~0.5 m beside the platform to avoid shaded temperature readings.

In 2015 a 4-rod ThetaProbe ML2x moisture probe was connected to the Auxiliary Sensor Interface in order to measure volumetric soil water content in sync with other LI-COR variables. Using a frequency of 100 MHz the probe transmits a signal into the soil to determine the apparent dielectric constant of the material, which is a function of the water content (Delta-T Devices, Ltd., 1999). The probe was inserted into a sedge hummock adjacent to the LI-COR platform (~1 m away).

3.2 Stable C and N Isotopes

The Picarro G2201-*i* analyzer measures $\delta^{13}C$ from CO_2 using cavity ring-down spectroscopy (CRDS). On July 8th, 2015 the analyzer was positioned along the boardwalk loop directly beside the LI-COR platform for a period of 3 hours in the early afternoon, powered by an 800 W Earthquake generator and 1000VA uninterrupted power source (UPS) backup battery system. Additional data collection in 2015 was performed in the afternoon/evening on the 6th of August (5 hours) and during an overnight period from August 27th-28th (9 hours), powered by a Subaru Industrial Portable generator and UPS for a lengthened measurement period. Restek stainless steel tubing (1/8" diameter) was connected to the distribution manifold and extended to collect measurements near the surface beside the LI-COR. An added seal of Teflon tape and subsequent breath tests ensured there were no leaks at the tubing connection point. LI-COR data also supplemented Picarro timelines at an increased resolution of 10-15 minute measurement intervals.

Soil isotope data were determined in the laboratory from a peat core collected near the boardwalk loop. In early spring of 2015, prior to the final surface thaw, a roughly cylindrical 27 cm deep (not including 10 cm of uncompact living/dead plant material at the surface, and 15 cm

of living plant material extruding from the surface) sample was removed using a chainsaw. At 5 cm depth intervals (beginning with plant material extruding from the surface) both plant/root and soil samples (~0.5 g each) were removed from the column and dried at 80 ºC overnight. After samples were devoid of moisture they were pulverized in liquid nitrogen using mortar & pestle, weighed in tin capsules, and run in an Elementar VisION Isotope Ratio Mass Spectrometer and Elemental Analyzer (IRMS-EA) to determine carbon and nitrogen isotope content.

3.3 Weather Station

University Field Station weather equipment is located in an open field approximately 1.2 km northwest of the Cedarburg Bog boardwalk loop. Records consist of continuous 30-minute intervals of barometric pressure (Campbell Scientific SBP270 barometer) measured in millibar (converted to kPa), atmospheric temperature in degrees Celsius and percent relative humidity (Campbell Scientific CS500 probe), radiation in kilowatt per square meter (LI-COR LI200X pyranometer), precipitation in millimeters (OTT Pluvio^2 rain gauge), and wind speed in meters per second (Campbell Scientific R. M. Young Wind Sentry-03001). Data were tracked and stored with a Campbell Scientific CR3000 Datalogger with the exception of a five-day period in early November 2014 (7^{th}-11^{th}) during equipment software updates. Although barometric pressure data are available from LI-COR chamber measurements, weather station pressure data are utilized in this study on the basis of measurement continuity.

3.4 Groundwater Monitoring

A Solinst Levelogger Edge transducer was kept in a monitoring well roughly 10 m from the LI-COR platform along the string bog boardwalk, recording water column pressure (m) at regular intervals (2014: 10-30 minutes, 2015: 60 minutes). The transducer hung from a 2 m long

string below a 0.71 m well casing, recording data at a depth of 1.29 m beneath the surface. Both elevation and zero point-offset corrections were accounted for according to the Solinst Levelogger User Guide (Solinst, 2015). Atmospheric pressure readings from the Cedarburg Bog Field Station were used for pressure correction.

Visual observations of groundwater trends in the string bog region were alarmingly different from monitoring well recordings. Upon further literature search, similar observations were found in an archived field station bulletin (Reinartz, 1985). The concern of a mobile peat surface in the string bog prompted additional investigation. As a simple solution, two Moultrie M-550 Gen2 trail cameras were placed on the boardwalk, recording 7 megapixel resolution images every 6 hours around 1 and 7 am/pm. From May – November of 2016 each camera was set to record images of the water/peat surface relative to 1) an anchored and ruled marked post (Figure 4a), and 2) the monitoring well casing (Figure 4b).

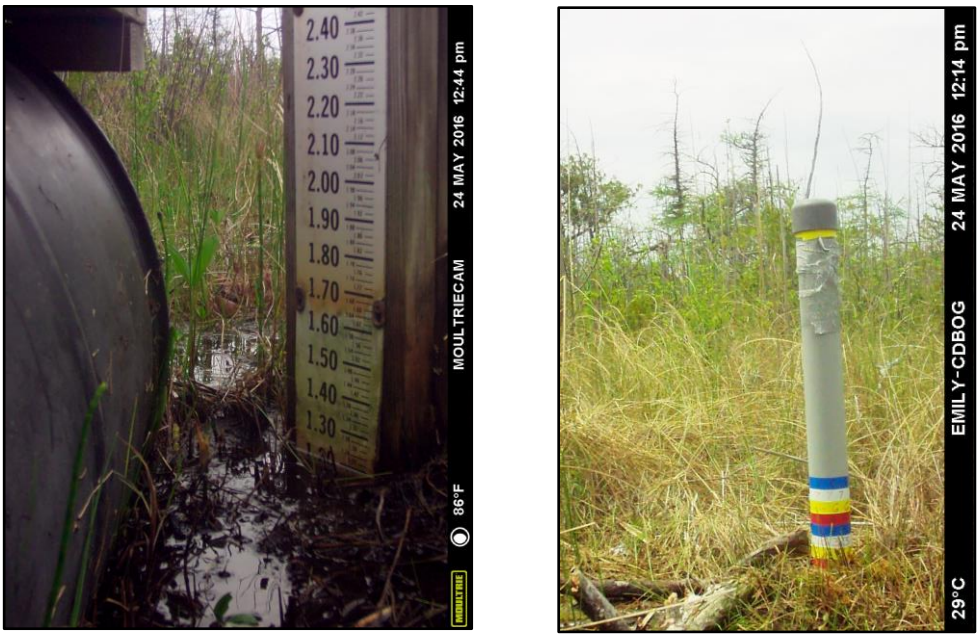

(a) (b)

Figure 4: Moultrie M-550 Gen2 trail camera locations recording (a) an anchored and marked post on the south end of the Boardwalk Loop, and (b) the groundwater monitoring well on the east end of the Boardwalk Loop.

3.5 JMP

Hypothesized relationships between surface CO_2 concentration, soil CO_2 flux, and external parameters (soil temperature and moisture, weather data) were addressed using the SAS statistical software program JMP. Using JMP, basic statistics such as averages and distributions were produced for each variable. In an attempt to account for the variation of multiple parameters influencing soil CO_2 flux and surface CO_2 concentration, multiple linear regression models were developed to support theoretical correlations.

3.6 Quality Control

Instruments used in the field were on occasion subject to conditions beyond the operation threshold designated by the manufacturer. Data have been filtered to exclude recordings made during these periods. In total, LI-COR recordings compile 7,872 data points, with data removed

based on the following criteria: i) chamber relative humidity > 95% (1.2%), ii) curve fit status error (0.2%), and iii) negative CO_2 flux (0.7%). While negative soil CO_2 flux calculations are not inherently incorrect, they are most likely the result of a leak in the instrument chamber while closed.

4. Results

4.1 Distribution of Soil CO_2 Flux

The intensity of soil CO_2 flux is broadly distributed across the entire data set. Flux was always positive, ranging from less than 1 to over 650 $mgCO_2/min\text{-}m^2$. Average for all CO_2 flux measured was 6.49 $mg/min\text{-}m^2$, with a median of 3.39 $mg/min\text{-}m^2$. A review by Oertel et al. 2016 highlighted studies of soil respiration in various environments providing similar results: in a temperate wetland, soil respiration averaged 6.73 $mgCO_2/min\text{-}m^2$; in a subtropical constructed wetland, soil respiration averaged 6.26 $mgCO_2/min\text{-}m^2$; other studies in the review averaged higher or lower rates of soil respiration (11.80 $mgCO_2/min\text{-}m^2$ in natural wetlands, and 5.28 $mgCO_2/min\text{-}m^2$ in a tropical wetland). A Minnesota peatland study measured soil CO_2 flux in hummocks and hollows and revealed averages of 6.81 and 3.75 $mg/min\text{-}m^2$, respectively (Kim and Verma 1992). These ranges highlight the tendency of soil CO_2 flux to be both temporally and spatially variable.

Figure 5 illustrates the frequency distribution of soil CO_2 flux intensity collected in this study, the corresponding day and night percentages, and the contribution of each to the total mass of CO_2 respired from the soil. Data were divided into three categories: i) < 5 $mgCO_2/min\text{-}m^2$ (low flux), ii) 5-50 $mgCO_2/min\text{-}m^2$ (medium flux), and iii) > 50 $mgCO_2/min\text{-}m^2$ (high flux). Ranges were selected according to the distribution of measurement frequency, which decreased exponentially at 5 and 50 $mg/min\text{-}m^2$. The inner pie chart in Figure 5 represents the

corresponding mass of soil respired CO_2. The total mass of soil respired CO_2 over the study period (1,915 gCO_2/m^2) was determined by integrating each measurement over the time between measurements (typically 30 min. in 2014 and 60 min. in 2015). This approach was taken based on the observation that CO_2 flux intensity most often increased and decreased similar to a normal distribution curve (as opposed to isolated events). It is recognized that the integration of CO_2 flux over 30 and 60 min. periods may be an under- or overestimation of total CO_2 mass, but this is the limit of the time resolution measured. Low flux occurred 71.1% of the time, and high flux occurred 1.4% of the time, each contributing a comparable amount to the mass of CO_2 respiring from the soil (28.4% and 23.0%, respectively). Medium flux occurred 27.5% of the time, and supported 48.6% of total CO_2 mass respired from the soil. Low flux showed no diurnal periodicity; 50.9% occurred during the day, and 49.1% occurred overnight. Medium and high flux typically occurred during the day (medium flux 77.0% and high flux 75.2%).

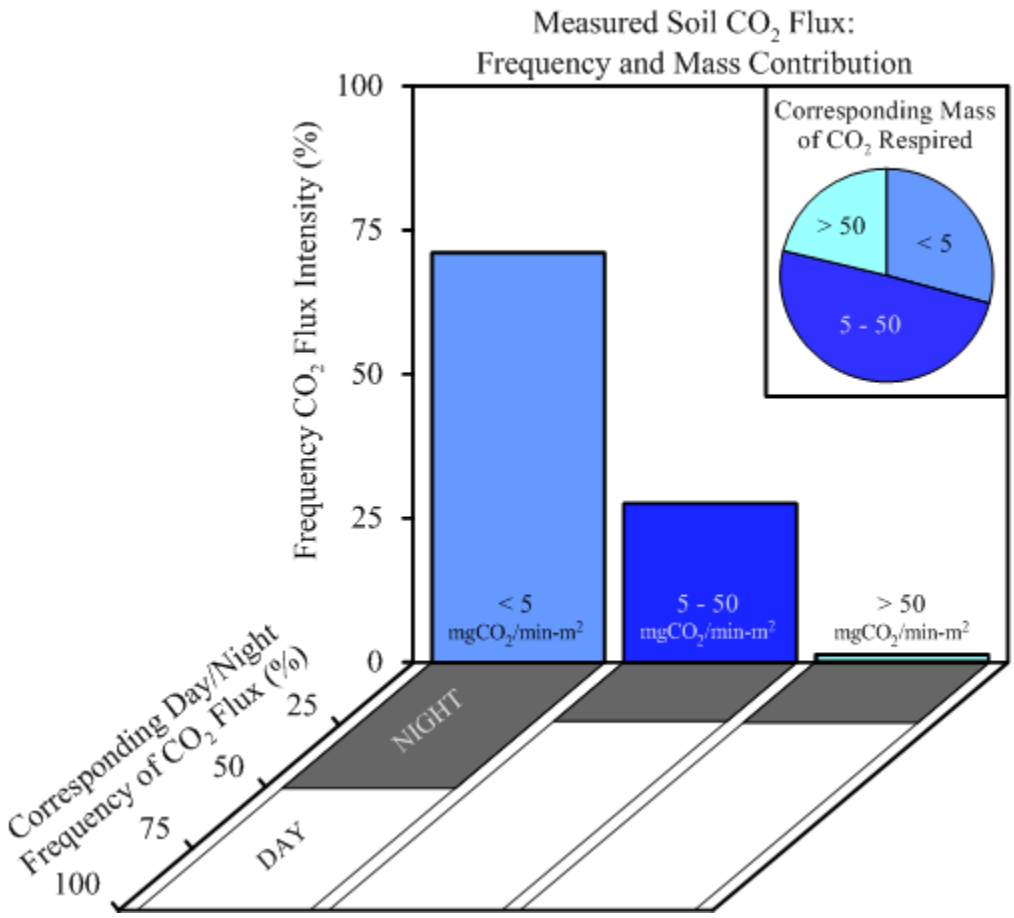

Figure 5: Bar charts showing distribution of soil CO_2 flux intensity based on entire data set (2014 & 2015) and subsequent percentages occurring during day/night periods (day: radiation > 0, night: radiation = 0). Inner pie chart represents the mass of CO_2 contributed by each bar to total soil respiration.

4.2 Diurnal and Seasonal Variations of CO_2

Surface CO_2 concentration typically illustrates distinct diurnal trends where concentration increases overnight and decreases during the day. In the majority of measurements, soil CO_2 flux trends are inverse to surface CO_2 concentration; this was investigated in detail during one overnight period from July 9th-10th, 2014, where LI-COR data were collected at 3-minute intervals. Figure 6a illustrates the frequency of this trend, where increased soil CO_2 flux more often occurred during the day, and increased surface CO_2 concentration occurred more often overnight.

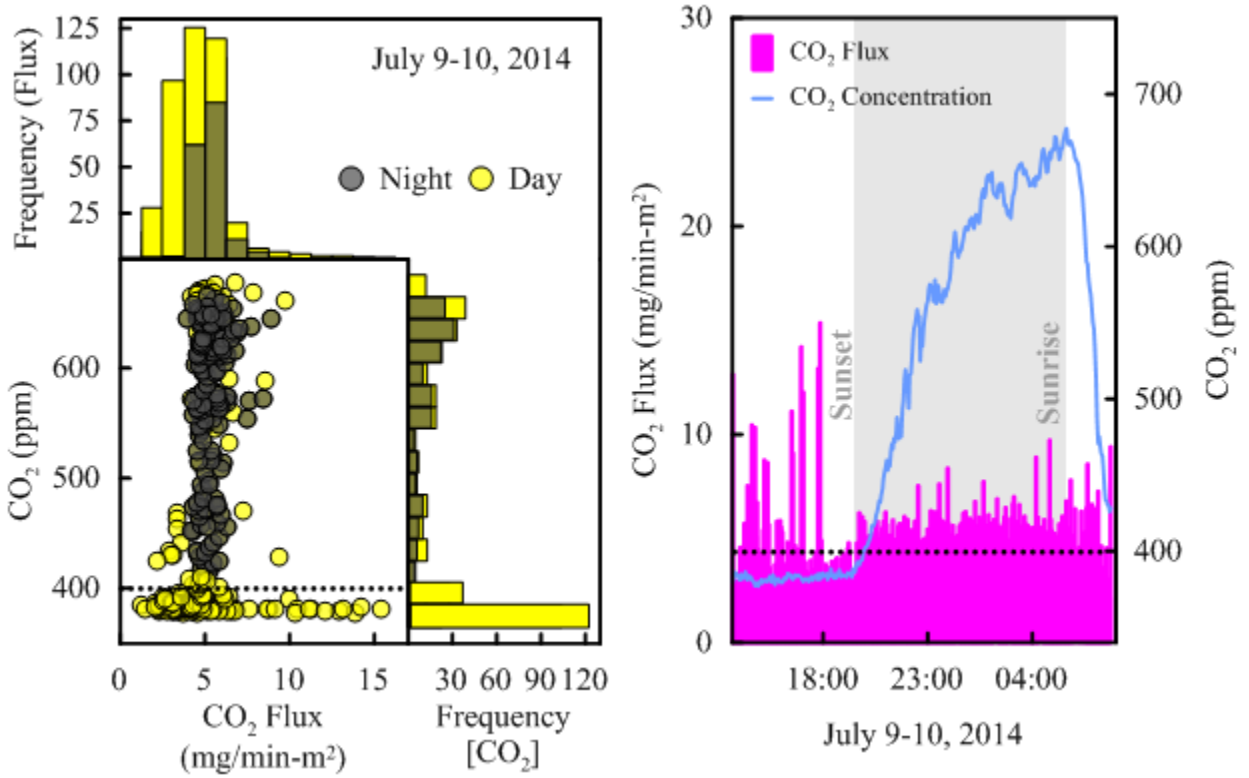

Figure 6: (a) Diurnal distribution of soil CO_2 flux and surface CO_2 concentration collected at 3 minute intervals (bars overlying, not stacked) and (b) corresponding timeline of data (July 9th-10th, 2014). Dotted lines represent average atmospheric CO_2.

The diel periodicity of surface CO_2 concentration expands seasonally; from spring to summer CO_2 concentration range increases, and from summer to fall CO_2 concentration range decreases (Figure 7a). This is evident across the entire data set, as represented in Figure 7b, which illustrates seasonal changes with soil temperature. Measured weather parameters including wind speed, radiation, and atmospheric temperature are typically out of phase with diel changes in surface CO_2 concentration.

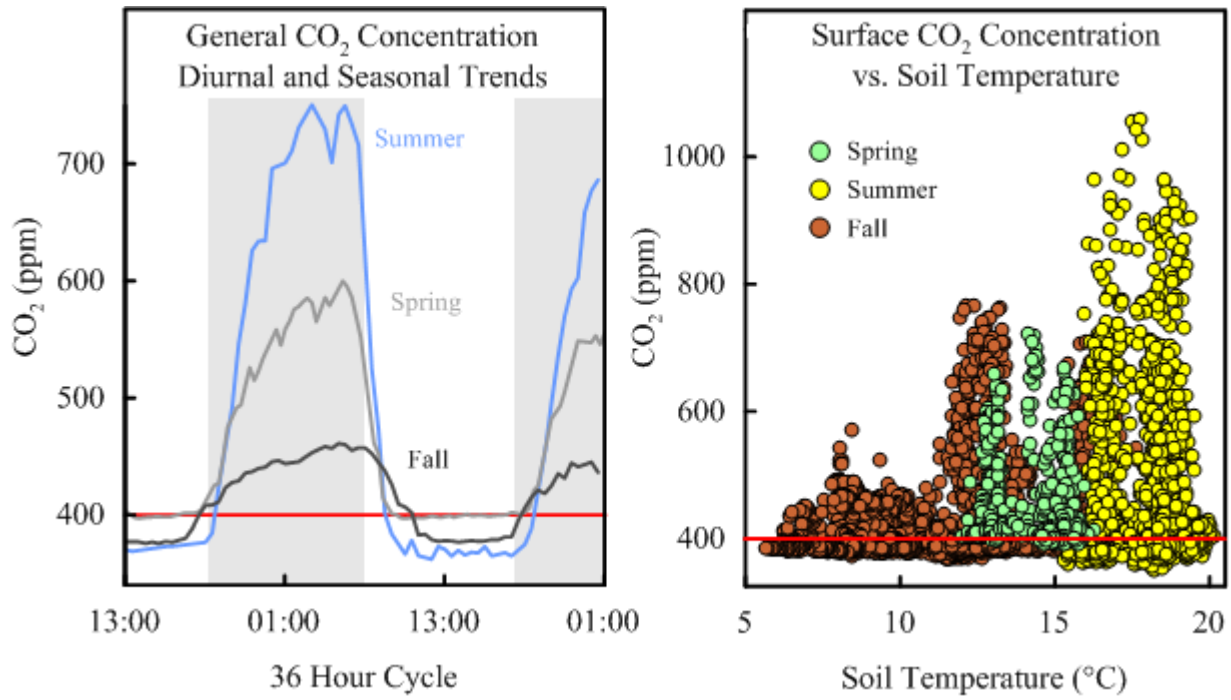

(a) (b)

Figure 7: (a) General diurnal and seasonal 36-hour trends of surface CO_2 concentration. Spring: May 23-25, 2014. Summer: Aug. 6-8, 2014. Fall: Oct. 21-23, 2014. Shaded bars represent overnight periods. (b) Seasonal soil temperature and surface CO_2 concentration changes. Red lines represent average atmospheric CO_2.

4.3 Correlations to Soil CO_2 Flux

Trends in soil CO_2 flux are less consistent in diurnal and seasonal variation compared to that of surface CO_2 concentration. Soil CO_2 flux typically increases during the day (Figure 5), adding to the low flux that occurs both day and night. Figure 8 presents a tyipcal example of the variation in soil CO_2 flux through time. Atmospheric temperature, radiation, and wind speed all vary in phase with the diurnal pattern of soil CO_2 flux (Figure 9a, b), while surface CO_2 concentration is typically out of phase (Figure 9b). The immensity of data collected in this study makes a bulk correlation approach unrealistic. Instead, data were broken down into categories (i.e. range of soil CO_2 flux intensity, day vs. night, environmental conditions) in an attempt to reveal correlations that might otherwise be masked by the large amount of variability observed across the entire data set.

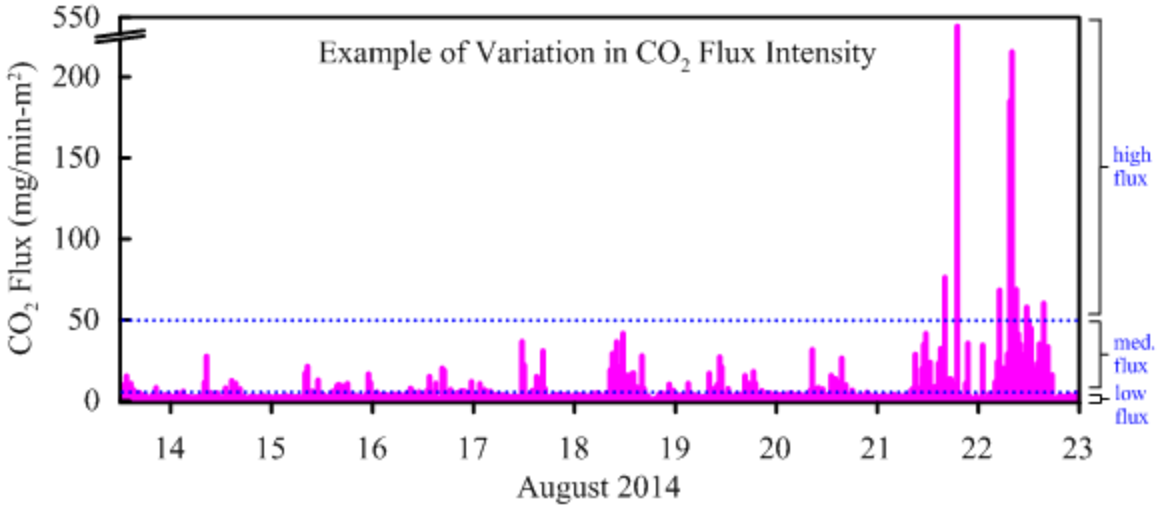

Figure 8: Example of variation in soil CO_2 flux intensity in the Cedarburg Bog from August 14 – 23, 2014. Dotted lines represent flux categories (< 5/low flux, 5 – 50/medium flux, > 50/high flux). Note break in y-axis.

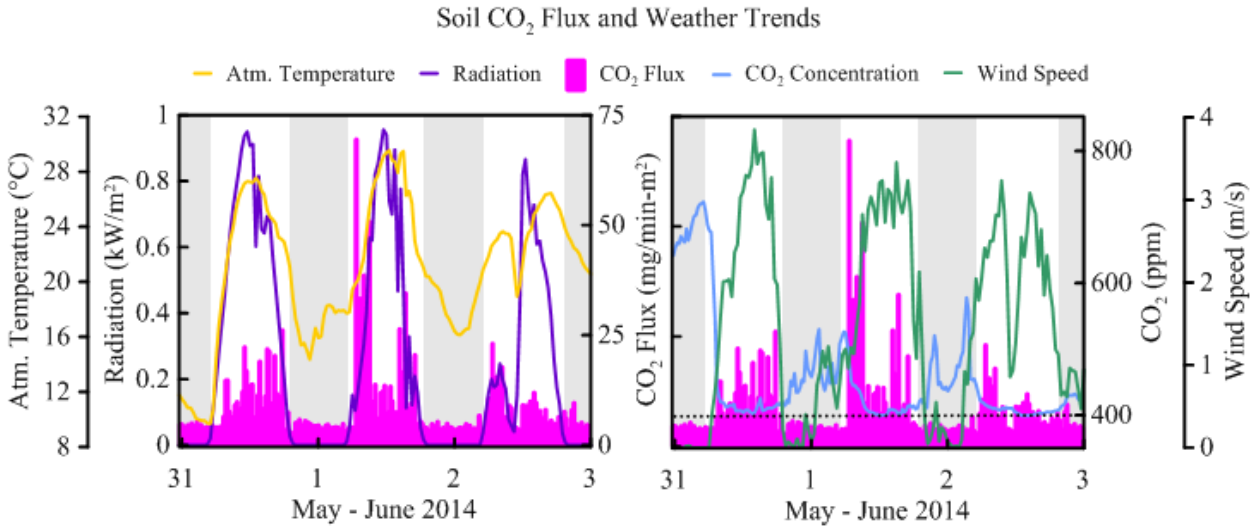

(a) (b)

Figure 9: Soil CO_2 flux trends alongside (a) atmospheric temperature and radiation, and (b) wind speed and surface CO_2 concentration, highlighting diurnal variation during May 31 – June 3, 2014. Shaded bars represent overnight periods. Dashed line represents average atmospheric CO_2.

Based on a linear regression model produced in JMP, soil temperature alone can account for 27.6% of the variation in low flux. Overnight (radiation = 0), 41.7% of low flux can be accounted for with soil temperature, surface CO_2 concentration, wind speed, and atmospheric temperature. Medium flux is poorly correlated; wind speed, surface CO_2 concentration,

atmospheric temperature, and precipitation can account for 2.3% of variation in medium flux. Wind speed can account for 1.7% of medium flux during the day, and 22.6% by soil and atmospheric temperatures overnight. No significant correlations were found using JMP when addressing high flux. An inclusive list of model inputs and results can be referenced in Appendix B.

4.4 Correlations to Surface CO_2 Concentration

CO_2 concentration measured at the soil surface displays a strong diurnal cycle in response to radiation; decreasing as soon as radiation rises above zero during the day, and only increasing in the absence of radiation overnight (Figure 10). High surface CO_2 concentration also varies in response to wind speed above a threshold of roughly 1-2 m/s, regardless of time of day. These trends are apparent across the entire data set, as seen in Figure 11. The data points that fall outside of the binary relationship between surface CO_2 and radiation are transitional, caught near the day/night boundary and decrease over time (Figure 11a, arrow). A similar trend is apparent between wind speed and CO_2 concentration, where concentrations increase during calm, low wind conditions and decrease near the level of atmospheric CO_2 (400 ppm) in turbulent wind conditions.

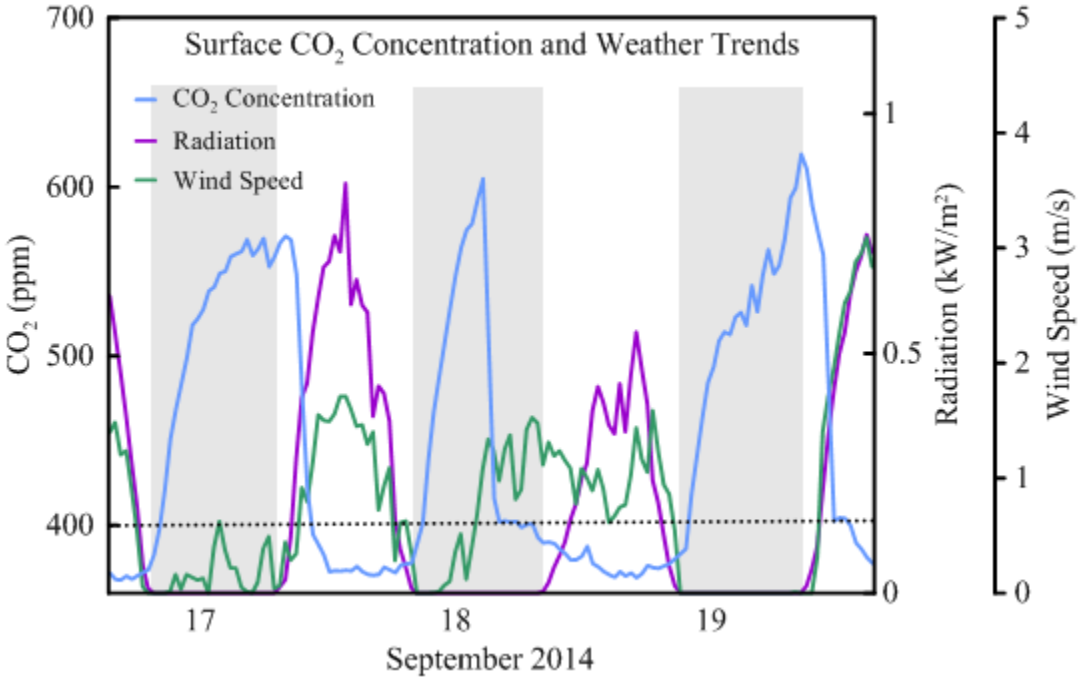

Figure 10: Surface CO_2 concentration trends alongside radiation and wind speed, highlighting out of phase diurnal variation for the period of September 16 – 19, 2014. Shaded bars are overnight periods. Dashed line represents average atmospheric CO_2.

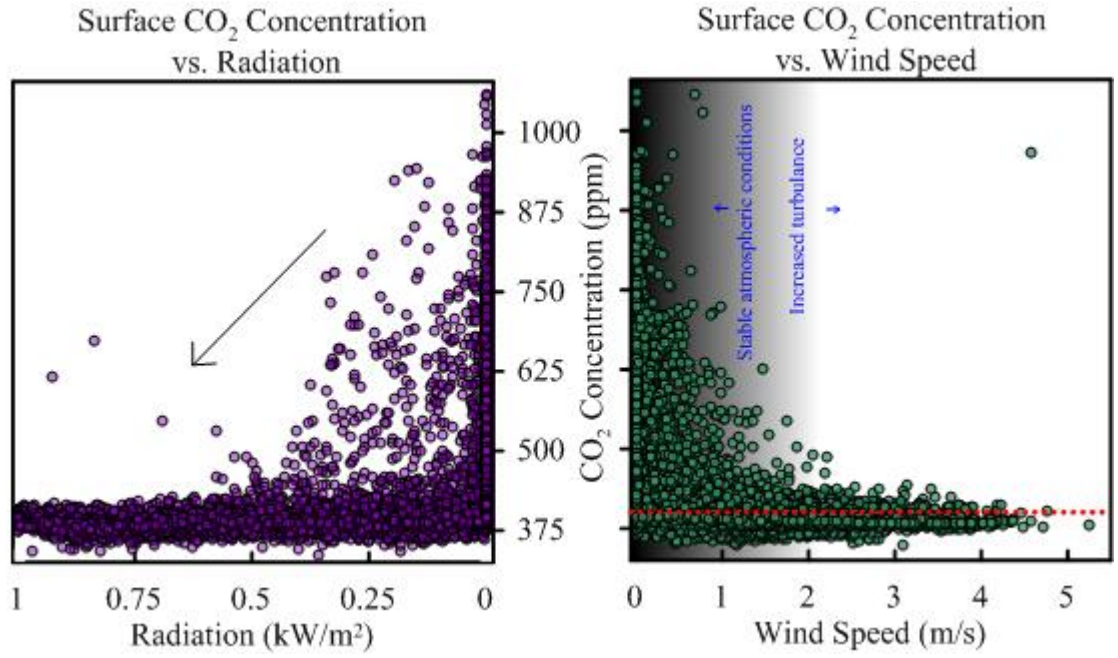

(a) (b)

Figure 11: (a) Surface CO_2 concentration and radiation, and (b) surface CO_2 concentration and wind speed for entire data set (2014 and 2015). Arrow represents transition of decreasing CO_2 concentration with onset of radiation. Red line represents average atmospheric CO_2.

Multiple linear regression models reveal that wind speed, soil temperature, radiation, atmospheric temperature, and soil moisture content can account for 30.7% of variation in surface CO_2 concentration. During the day (radiation > 0), wind speed, atmospheric temperature, and soil temperature can account for 22.8% of surface CO_2; overnight, wind speed and soil temperature can account for 29.7% of variation in surface CO_2 concentration. When wind speed < 2 m/s (assumed calm conditions), wind speed, soil temperature, atmospheric temperature, and radiation can account for 34.0% of CO_2 concentration variation. For surface CO_2 concentration > 400 ppm (average atmospheric CO_2), wind speed and soil temperature can account for 22.6% of CO_2 concentration variation, and for concentrations < 400 ppm, atmospheric temperature, soil moisture content, and wind speed can account for 13.9% of variation in surface CO_2 concentration.

4.5 Stable Isotope Signatures

Peat core samples show carbon isotope signatures of root and peat material converging between 5 and 20 cm beneath the compact peat surface (Figure 12). At this depth, root biomass $\delta^{15}N$ signatures are ~0 ‰. Considering the signature of atmospheric $\delta^{15}N$ remains consistently near 0 ‰ (Fry 2008), and that bacteria utilize atmospheric nitrogen in decomposition, the depth at which 0 ‰ $\delta^{15}N$ signatures were measured indicates the presence of nitrogen-fixing organisms (microbes). The range of $\delta^{13}C$ at the same depth suggests a $\delta^{13}C$ microbial biomass signature to be between -19 and -22 ‰.

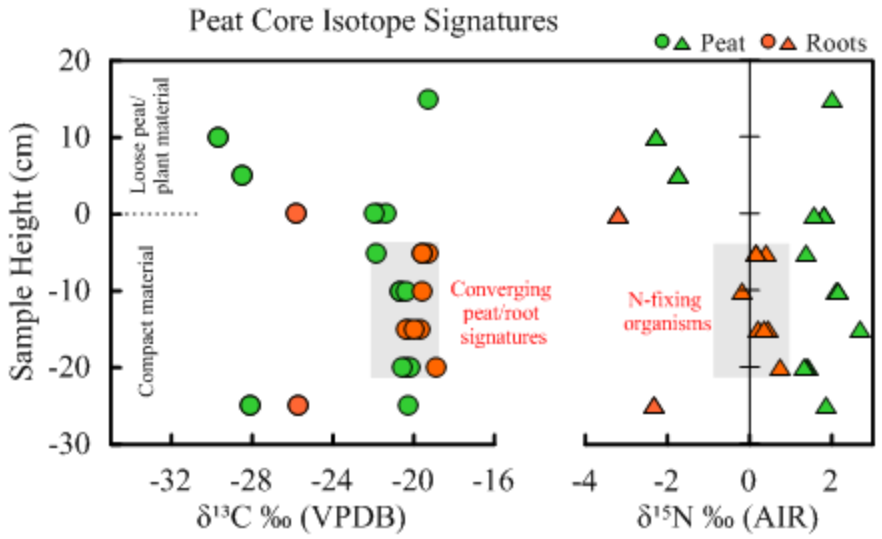

Figure 12: Cedarburg Bog peat core depth profile of IRMS-EA stable isotope signatures. Circles represent $\delta^{13}C$ signatures, triangles represent $\delta^{15}N$ signatures. 'Peat' (green) represents organic material beneath the surface, or plant material above the surface. 'Roots' (red) represents root material sampled at/beneath the surface. Shaded boxes represent depth of inferred microbial activity. (image modified from Erik Gulbranson 2015)

Carbon isotope signatures from gaseous CO_2 collected with the Picarro stable isotope analyzer were interpreted for CO_2 source signatures using Keeling plot analyses. Keeling plots are based on conservation of mass, with the assumption that measured $\delta^{13}C$ of CO_2 is a mix of two different end members (background and source). Plotting the inverse of concentration against $\delta^{13}CO_2$ signatures displays the two end members on a linear regression line, the intercept of which represents the source component signature in the absence of background concentration (Pataki et al. 2001).

Each Picarro measurement period consisted of different collection criteria (i.e. time of day, measurement interval). This resulted in a wide range of $\delta^{13}CO_2$ source signatures from Keeling plot analyses. Data from July 8, 2015 and Aug. 6, 2015 Picarro measurement periods produced poor correlations in Keeling plot analyses (R-square of 0.002 and 0.09, respectively), and so are not used as representative signatures for soil respired CO_2. The period of Aug. 27-28,

2015 produced strong correlation to the regression line (R-square 0.97, Figure 12b). In this Keeling plot, the background end member is atmospheric $\delta^{13}CO_2$, and the intercept soil respired $\delta^{13}CO_2$. From the Keeling plot analysis, the $\delta^{13}C$ of soil respired CO_2 (y-intercept) is estimated to be -21.9 ‰. Figure 12a shows the transition between end members in time; more turbulent conditions during the day resulted in a stronger atmospheric $\delta^{13}C$ signal, and moved towards a signal of soil respired $\delta^{13}C$ during the calm overnight period. Furthermore, these end member signatures are consistent with literature $\delta^{13}C$ signatures for atmospheric (~ -8 ‰) and terrestrial (~ -23 ‰) CO_2 (Lajtha and Michener 1994; Sharp 2007).

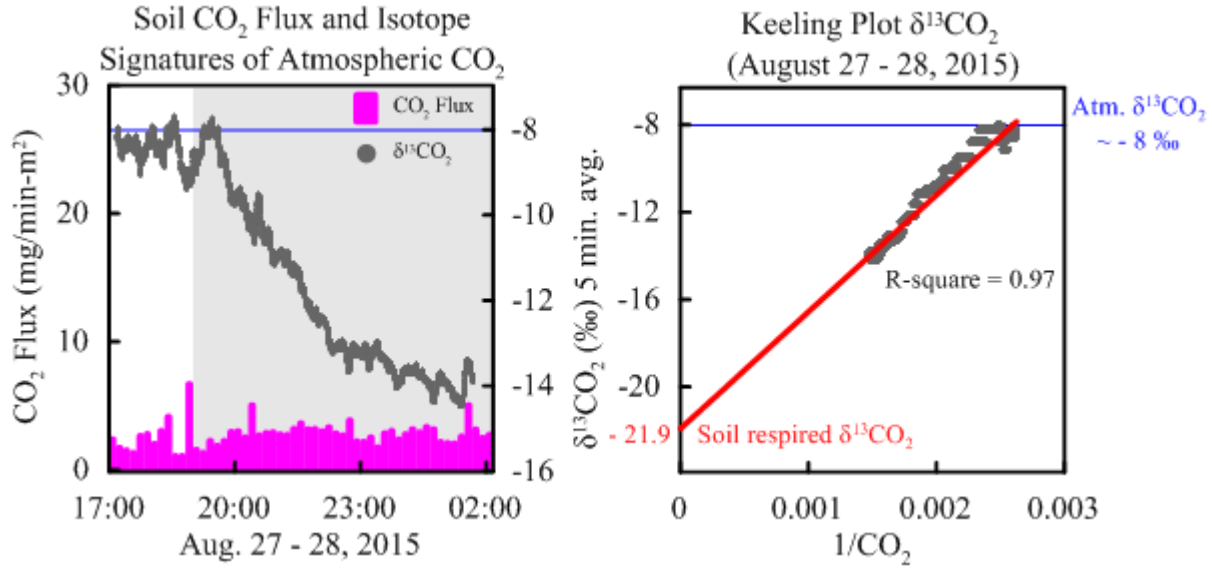

Figure 13: (a) LI-COR soil CO_2 flux and Picarro $\delta^{13}CO_2$ of atmospheric CO_2 27-28 August 2015 in the Cedarburg Bog and (b) corresponding Keeling plot with intercept of -21.9 ‰ (R-square 0.97). Blue lines represents atmospheric $\delta^{13}CO_2$. Shaded box represents overnight period.

4.6 Water Table and Peat Surface Trail Camera Observations

Field notes during the second field season of this study (2015) describe the water table in the string bog region of the Cedarburg Bog remaining at or above the peat surface. However, transducer data collected from the boardwalk loop monitoring well did not reflect this

observation. A UW-Milwaukee Field Station Bulletin detailing the various wetland characteristics of the Cedarburg Bog also notes the difference in the "apparent" water table fluctuation in the string bog region compared to that of surrounding habitats (Reinartz 1985). In one survey, the Bog water level was observed to fluctuate almost 50 cm, while the string bog water level appeared to vary within only 15 cm. It has been suggested that the low nutrient and oxygen availability in the string bog inhibits plants from developing deep root zones. If the peat layer is unanchored by deeper root systems, it may be subject to movement with the rise and fall of the water table as a loose and expandable mat. Grittinger 1971 made a similar observation, noting that the string bog mat was "very soft and treacherous to tread upon, and though it appears to float, seems to lack some of the resiliency of the emergent aquatic mat."

The two trail cameras placed in the string bog in 2016 showed the peat surface subsiding as much as 12 cm from May – August (Figure 14). While these changes cannot be extrapolated to represent changes in water table elevation during the study periods of 2014 and 2015, they confirm that the elevation of the peat surface in the string bog is not constant. The theoretical correlation between groundwater level and soil CO_2 flux is based on an increase in oxygen content when the water table lowers, thus increasing CO_2 emission (IPCC 2013). Because the transducer pressure data are corrected based on a specific elevation datum, the uncertainty in elevation of the peat surface relative to the water table makes the groundwater data ineffective for correlation with soil CO_2 flux.

(a) (b)

Figure 14: Trail camera observations of the boardwalk loop monitoring well in the string bog region of the Cedarburg Bog showing the subsidence of peat surface; May 20, 2016 (a) and Aug. 11, 2016 (b). Colored bands are 1.8 cm thick.

5. Discussion

Soil respiration studies often rely on data sets of limited temporal frequency (i.e. one measurement per day for several days, or several measurements weekly or monthly). Due to the large range of soil CO_2 flux intensity, especially on a diurnal cycle, studies relying on limited measurements provide biased results, and subsequent models therefore over- or underestimate predicted soil CO_2 flux. In addition, a review by Kuzyakov and Gavrichkova 2010 warned of the potential for studies to neglect controls that trend similarly in time. Atmospheric temperature, for example, co-varies with radiation, though most studies consider only the influence of temperature, and not that of radiation. Failure to account for influential variables affecting soil CO_2 flux also creates estimates that poorly represent actual conditions. This study presents an

unparalleled high-resolution temporal data set of wetland soil CO_2 flux. Soil CO_2 flux is a function of multiple interdependent physical and biological processes; those presented here do not directly account for the entire variation of CO_2 flux, but provide significant insight to the extent of variation, and the controls of production and transport of soil CO_2.

Soil CO_2 flux is derived from both heterotrophic (microbial decomposition of organic matter) and autotrophic (root) respiration (Czimczik et al. 2006; Hanson et al. 2000; Hopkins et al. 2012; Kuzyakov and Gavrichkova 2010). Root respiration is a product of both root activity and microbial activity in the rhizosphere (the dynamic area where plant roots exchange nutrients with the soil), and is considered here to represent both of these influences collectively (Hanson et al. 2000). Therefore, the two main sources of soil respiration discussed in this study are 1) root respiration (including rhizo-microbial respiration), and 2) microbial respiration. The contribution of each source to soil CO_2 flux is dependent on the factors/processes controlling assimilation and release of CO_2 by the plants/microbes, and soil transport of CO_2 (Figure 15).

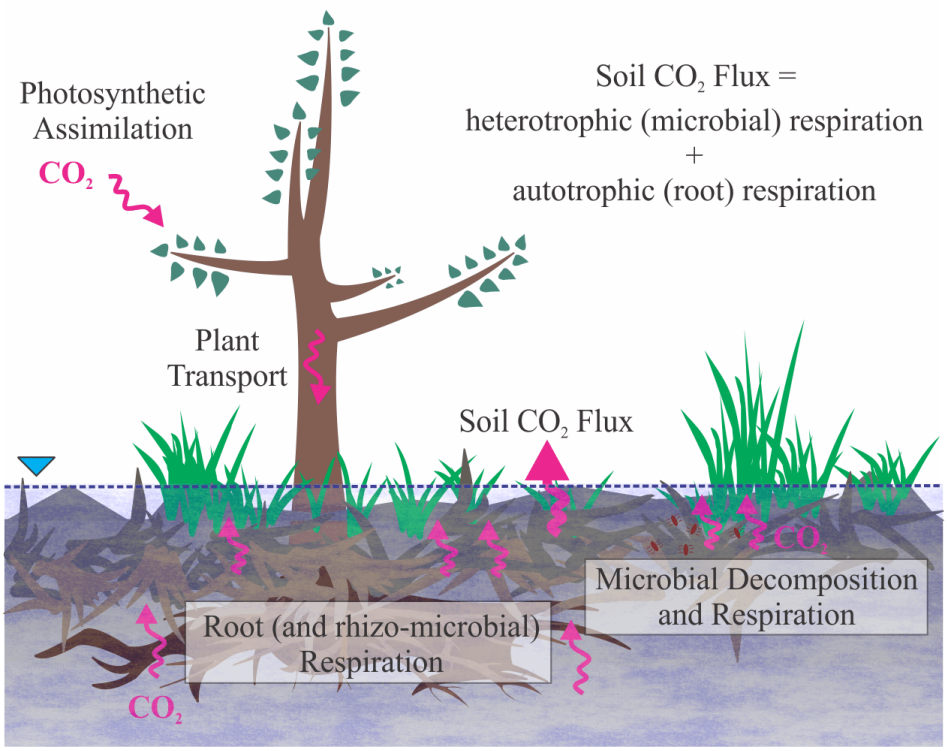

Figure 15: Root and microbe sources of soil respired CO_2 and aboveground input of CO_2 acquired via photosynthesis.

5.1 Microbial Respiration and Soil CO_2 Flux

Across both field seasons, a continual low flux was observed, regardless of time of day. This 'basal' respiration (Koerber et al. 2010), is the product of microbial respiration in the soil. This is supported by the isotope analyses of $\delta^{13}CO_2$ measured at the soil surface and of $\delta^{13}C$ and $\delta^{15}N$ from the peat core. The Keeling plot analysis of soil respired CO_2 measured Aug. 27-28, 2015 captured this basal respiration (Figure 13a), and revealed that soil respired CO_2 had an isotopic signature of -21.9 ‰ (Figure 13b). The sampled soil media from the extracted peat core revealed an approximate microbial biomass $\delta^{13}C$ of ~ -19 to -22 ‰ (Figure 12), confirming the source of low flux to be microbial respiration in the soil.

Rate of organic decomposition, and subsequent microbial production of CO_2 in the soil, is dependent on soil temperature, soil moisture, and nutrient availability (Inglett et al. 2012). In

the Cedarburg Bog, 27.6% of low flux can be directly accounted for by soil temperature. Soil saturation can be influential to decomposition rate, based on the level of oxygen available (aerobic vs. anaerobic conditions). The low oxygen availability in the string bog region of the Cedarburg Bog is evident in the perpetually waterlogged peat (Reinartz 1985). During the 2015 field season, soil moisture content was measured in the string bog, and revealed a nearly consistent level of saturation; volumetric water content = 0.61 ± 0.02 m^3/m^3. While soil moisture content is inherently influential to microbial productivity and subsequent soil respiration, the consistent level of saturation in the string bog region of the Cedarburg Bog minimalizes its influence to variation of soil CO_2 flux in this study.

5.2 Root Respiration and Soil CO_2 Flux

The timeline of Picarro measurements did not coordinate with increased rates of soil CO_2 flux that are attributed to root respiration (5 – 50 mg/min-m^2). However, it is assumed that if root respiration were apparent during the measurement period of Aug. 27-28, 2015 (Figure 13a), the source signature identified from the Keeling plot regression would be more depleted in $\delta^{13}C$ (more negative). From the living plant material sampled in the peat core (above the surface), plant biomass were near -28 to -30 ‰ (not including an anomalous sample near -19 ‰). Assuming little/no fractionation, root respired $\delta^{13}CO_2$ would be similar to the $\delta^{13}C$ signature of plant biomass.

Tracer studies have also illustrated the importance of root respiration to soil CO_2 flux, where isotopically labelled pulses of radioactive ^{14}C or stable ^{13}C are administered to a plant and measured later in soil respiration (Hanson et al. 2000). Root respired CO_2 is in part dependent on the assimilation of CO_2, performed above ground during photosynthesis. Photosynthesis is in turn dependent on photosynthetically active radiation (PAR), the availability of CO_2, and

temperature. The simultaneous fluctuation in atmospheric temperature and radiation often masks the influence of radiation to CO_2 assimilation and subsequent soil respiration. Either of these (radiation, CO_2, temperature) can act as a limiting factor in photosynthetic assimilation of CO_2, and so should be considered when addressing sources of total soil respiration.

In this study, a diurnal pattern of medium flux was often observed in response to increasing radiation and atmospheric temperature (Figure 9). This is attributed to root respiration in response to aboveground photosynthetic assimilation of CO_2, and is thus linked to processes separate from that of soil temperature and microbial respiration mentioned previously (Hopkins et al. 2012; Kuzyakov and Gavrichkova 2010). Following plant assimilation of CO_2 through photosynthesis, the response time of root respiration is variable depending on the transport mechanism used. Kuzyakov and Gavrichkova 2010 suggest two main transport mechanisms leading to root respiration: 1) direct transport and 2) indirect transport.

Direct transport moves nutrients from leaves to roots through the phloem, and although the assimilation of CO_2 in photosynthesis occurs within seconds, the time it takes for molecules to move through the plant depends largely on distance, or plant height. Transport rates typically range from 0.5 to 1 m/hr; the stunted cedar and tamarack trees, and the low sedge areas composing the string bog region are likely on the faster end of these averages. The second transport mechanism, indirect transport, relies on pressure concentration waves that occur several orders of magnitude faster than direct transport. Unlike direct transport, indirect transport is not the movement of molecules, but a concentration gradient that causes roots to release molecules they have already received. Though this mechanism occurs faster than direct transport, the duration of the resultant root respiration is shorter. Root respiration response to pressure

concentration waves, while significant, it is not considered as important to total root respiration as that of direct transport. (Gavrichkova and Kuzyakov 2012).

Multiple linear regression models were developed to address correlations between the range of soil CO_2 flux attributed to root respiration (medium flux) and variables driving photosynthetic assimilation of CO_2 (radiation, atmospheric temperature, surface CO_2 concentration). Although correlations between these variables are visually apparent (Figure 9), they were not reflected in JMP models. This is due to the missing variable of *time*. Multiple linear regression models did not account for the variation in time between CO_2 assimilation and subsequent root respiration. If transport mechanisms (direct or indirect) and rates of CO_2 transport are identified, a variable of time can be included in JMP models, and correlations would increase.

Finally, the time it takes for root or microbial respired CO_2 to diffuse through the soil/water column to the surface can be highly variable depending on the porosity and saturation of the soil (discussed further in 5.3), as well as the depth of production. The string bog region of the Cedarburg Bog may have a shallow rooting system (Reinartz 1985), therefore the depth of production may not be as limiting to response time as the physical structure of the peat. Based on a rate of medium flux, root respiration was estimated to contribute 48.6% of the total mass of soil CO_2 respired. This is similar to the study by Silvola et al. 1996, who estimated the contribution of root respiration to soil respiration in a peatland environment to be 35-45%.

5.3 Physical Controls of Soil CO_2 Flux

The rate at which CO_2 diffuses through the soil column is partly dependent on the physical structure of the soil; the permeability, tortuosity, porosity, and water content. It is

important to consider these properties when addressing soil CO_2 flux because gas diffuses several thousand times slower in water than in air (Sherwood et al. 2013). The upper layer of peat in the string bog region is a loose/expandable mat (see section 4.6), suggesting that these properties are not static. However, the soil moisture probe deployed during the 2015 field season revealed a nearly constant volumetric water content of 0.61 ± 0.02 m^3/m^3. It should be noted that although the soil moisture probe was placed near the LI-COR soil gas flux analyzer (~1 m), the vegetation and soil surface are highly spatially variable in this region. Thus, soil moisture conditions and the subsequent control on gas diffusion rate may also be variable over short distances.

Multiple studies have considered soil gas release via ebullition (bubbling) in response to decreasing atmospheric pressure (Tokida et al. 2005; Tokida et al. 2007; Waddington et al. 2009). The high solubility of CO_2 in water implies that the primary mechanism for CO_2 transport is diffusion, rather than ebullition. Still, the influence of atmospheric pressure was investigated in an attempt to explain irregular high flux measurements that were inconsistent with general trends of root and microbial respiration. When addressing the timeline of soil CO_2 flux data in accordance with atmospheric pressure, several periods demonstrate an increase in CO_2 flux intensity following decreasing atmospheric pressure. However, this is not observed exclusively, and the response in time and flux intensity, as well as the rate of falling atmospheric pressure, were highly inconsistent. A study on lake productivity of CO_2 and CH_4 by Casper et al. (2000) addressed ebullition in response to atmospheric pressure and revealed that 1% of CO_2 transport across the air-water interface was through ebullition, and the other 99% diffusion. Based on this, and the overall lack of immediate CO_2 flux response to decreasing atmospheric pressure, ebullition is an unlikely contributor to soil CO_2 flux in this study.

Precipitation is also suggested to act as a control of soil CO_2 flux; during precipitation events, CO_2 flux may be promoted through volumetric displacement of soil gas in air-filled pore space (LI-COR 2010). In the string bog region, the peat pore space remained more water-filled than air-filled (consistently saturated; and as previously discussed, CO_2 rarely moves advectively), thus precipitation as a physical force is not considered influential to soil CO_2 flux in this study.

The stark difference in intensity and frequency of high soil CO_2 flux suggests other mechanism(s) operating in addition to those mentioned previously. However, the parameters measured in this study did not account for this variation. These high-intensity soil CO_2 flux measurements are orders of magnitude above basal soil respiration, and although they occurred only 1.4% of the time, they account for 23.0% of CO_2 mass moving from the soil, and so are just as important to consider as low and medium ranges of flux. Furthermore, studies collecting only periodic, intermittent measurements of soil CO_2 flux risk either a) entirely missing this high rate of CO_2 flux or b) capturing this rate of CO_2 flux and subsequently overestimating CO_2 flux for that period.

LI-COR and weather measurements also provide insight to controls of surface CO_2 concentration, and could reveal a mass balance estimate of ecosystem respiration (source v. sink) if the height of the atmospheric boundary layer were determined. Overnight, when conditions are typically calm and no photosynthesis is occurring, CO_2 stratifies in the atmosphere, building at the soil surface (Figures 10, 11). During the day, as the rate of photosynthesis and wind turbulence increase, CO_2 concentration built up overnight becomes well mixed, and surface CO_2 concentration decreases to levels approximating atmospheric CO_2, which averages near 400 ppm (NOAA 2017). The rate at which CO_2 moves into or out of the ecosystem depends on the

difference in surface CO_2 relative to atmospheric CO_2, and the height of the atmospheric boundary layer.

6. Conclusions

Soil CO_2 flux can vary greatly over short periods of time. In the Cedarburg Bog, measurements ranged from less than 1 to over 650 $mgCO_2/min\text{-}m^2$. Studies that measure soil CO_2 flux at limited intervals risk misrepresenting the full range of CO_2 flux intensity, and risk creating biased models of soil CO_2 flux. This study presented an unparalleled high-resolution temporal data set of soil CO_2 flux in the Cedarburg Bog. Soil CO_2 flux is a function of multiple interdependent physical and biological processes; those presented in this study do not directly account for the entire variation of soil CO_2 flux, but provide significant insight to the extent of variation, the importance of high-resolution measurements, and the controls of production and transport of soil CO_2.

Net ecosystem exchange depends on the balance between soil respiration, above ground respiration, and photosynthetic assimilation. In the Cedarburg Bog, soil respiration in 2014 and 2015 resulted in a total soil CO_2 flux of 1,915 gCO_2/m^2, or ~2,200 $kgCO_2$ throughout the entire string bog area (~1.2 km^2). Sources of soil CO_2 flux include microbial respiration and root (including rhizo-microbial) respiration. Basal soil respiration (low flux) is the result of microbial respiration and provides a continual source (day and night) of CO_2. Microbial respiration trends partly mimicked soil temperature; 27.6% of the variation in low flux could be directly accounted for by changes in soil temperature. Although basal respiration occurred the vast majority of the time (71.1%), it contributed a relatively small percent (28.4%) of the total mass of CO_2 respired from the soil.

Root respiration largely depends on photosynthetic assimilation of CO_2 above the surface, and as such was associated with the diurnal cycle of medium flux. The contribution of root respiration to soil CO_2 flux is dependent on the rate of photosynthesis, which is in turn dependent on radiation, atmospheric temperature, and CO_2 availability, as well as plant transport mechanisms. Determining plant transport times leading to root respiration would increase correlations between variables controlling photosynthesis and the resultant medium soil CO_2 flux from root respiration. In assessing the mass of CO_2 moving from the soil, root respiration is especially important to consider, as it contributes just under half (48.6%) of total CO_2 respired from the soil.

The range of infrequent high flux (only 1.4% of measurements) is poorly understood. It was hypothesized that high flux is controlled by atmospheric pressure (ebullition), precipitation (volumetric displacement), and/or water table elevation (oxic layer boundary conditions). None of these variables were correlated, but the occurrence of high flux remains of great importance as it contributed 23.0% of the mass of CO_2 moving from the soil.

Soil respiration is a function of multiple interdependent physical and biological parameters. In order to improve predictions of wetland CO_2 dynamics in a changing climate, these relationships and the models produced to represent them must be improved. In this study, numerous variables were measured in anticipation of correlation to soil CO_2 flux; multiple linear regression models revealed weak and significant correlations due to missing variables of transport/response times. Wetland soils are structurally complex, and can be highly variable through time; improving correlations for soil respiration models requires high-resolution data sets, and determination of lag/response times of CO_2 transport processes above ground and in the soil.

References

Brooker, M.R., Bohrer, G., Mouser, P.J. (2014). "Variations in potential CH_4 flux and CO_2 respiration from freshwater wetland sediments that differ by microsite location, depth and temperature." *Ecological Engineering*. 72: 84-94.

Casper, P., Maberly, S.C., Hall, G.H., Finlay, B.J. (2000). "Fluxes of methane and carbon dioxide from a small productive lake to the atmosphere." *Biogeochemistry*. 49(1): 1-19.

Comas, X., Kettridge, N., Binley, A., Slater, L, Parsekian, A., Baird, A.J., Strack, M., Waddington, M. (2014). "The effect of peat structure on the spatial distribution of biogenic gases within bogs." *Hydrological Processes.* 28: 5483-5494.

Czimczik, C.I., Trumbore, S.E., Carbone, M.S., Winston, G.C. (2006). "Changing sources of soil respiration with time since fire in a boreal forest." *Global Change Biology*. 12(6): 957-971.

Darenova, E., Pavelka, M., Macalkova, L. (2016). "Spatial heterogeneity of CO_2 efflux and optimization of the number of measurement positions." *European Journal of Soil Biology*. 75: 123-134.

Dinsmore, K.J., Billett, M.F., Dyson, K.E. (2013). "Temperature and precipitation drive temporal variability in aquatic carbon and GHG concentrations and flux in a peatland catchment." *Global Change Biology*. 19: 2133-2148.

Fry, Brian. (2008). Stable Isotope Ecology. 3rd Edition. Spring Science+Business Media, New York, New York.

Gavrichkova, O., Kuzyakov, Y. (2012). "Direct phloem transport and pressure concentration waves in linking shoot and rhizosphere activity." *Plant Soil*. 351: 23-30.

Goffin, S., Aubinet, M., Maier, M., Plain, C., Schack-Kirchner, H., Longdoz, B. (2014). "Characterization of the soil CO_2 production and its carbon isotope composition in forest soil layers using the flux-gradient approach." *Agricultural and Forest Meteorology*. 188:45-57.

Görres, C.M., Kammann, C., Reinhart, C. (2016). "Automation of soil flux chamber measurements: potentials and pitfalls." *Biogeosciences*. 13: 1949-1966.

Graham, Jackson, "Climate Impact on Groundwater Flow Processes in the Cedar Creek Watershed and Cedarburg Bog" (2015). Theses and Dissertations. University of Wisconsin-Milwaukee. Paper 951.

Grittinger, T.F. (1970). "String Bog in Southern Wisconsin." *Ecology*. 51(5): 928-930.

Grittinger, T.F. (1971). "Vegetational Patterns and Ordination in Cedarburg Bog, Wisconsin." *Wisconsin Academy of Sciences, Arts and Letters.* 59: 79-106.

Gulbranson, Erik. (2015). Figure 12 modification. Personal communication.

Han, Weon Shik. (2015) Figure 2 modification. Personal communication.

Hanson, P.J., Edwards, N.T., Garten, C.T., Andrews, J.A. (2000). "Separating Root and Microbial Contributions to Soil Respiration: A Review of Methods and Observations." *Biogeochemisty*. 48: 115-146.

Hashimoto, S., Komatsu, H. (2005). "Relationships between soil CO_2 concentration and CO_2 production, temperature, water content, and gas diffusivity: implications for field studies through sensitivity analyses." *Journal of Forest Research.* 11: 41-50.

Hopkins, F., Gonzalez-Meler, M.A., Flower, C.E., Lynch, D.J., Czimczik, C., Tang, J., Subke, J.A. (2013). "Ecosystem-level controls on root-rhizosphere respiration." *New Phytologist*." 199(2): 339-351.

Inglett, P.W. Reddy, K.R., Corstanje, R. (2005). "Anaerobic Soils." *Encyclopedia of Soils in the Environment*. 72-78.

IPCC 2014, 2013 Supplement to the 2006 IPCC Guidelines for National Greenhouse Gas Inventories: Wetlands, Hiraishi, T., Krug, T., Tanabe, K., Srivastava, N., Baasansuren, J., Fukuda, M. and Troxler, T.G. (eds). Published: IPCC, Switzerland.

Kim, J., Verma, S. (1992). Soil Surface CO2 Flux in a Minnesota Peatland. *Biogeochemistry*. 18(1), 37-51.

Kline, J. (1991) "Vascular Plants of the Sapa Bog." University of Wisconsin-Milwaukee. Field Station Bulletin: 24(1).

Koerber, G.R., Hill, P.W., Edwards-Jones, G., Jones, D.L. (2010). "Estimating the component of soil respiration not dependent on living plant roots: Comparison of the indirect y-intercept regression approach and direct bare plot approach." *Soil Biology and Biochemistry*. 42(10): 1835-1841.

Kuzyakov, Y., Gavrichkova, O. (2010). "Time lag between photosynthesis and carbon dioxide efflux from soil: a review of mechanisms and controls." *Global Change Biology*. 16: 3386-3406.

Lajtha, K., Michener, R.H. (1994). Methods in Ecology: Stable Isotopes in Ecology and Environmental Science. Blackwell Scientific Publications,. Osney Mead, Oxford.

Lee, M.S., Nakane, K., Nakatsubo, T., Mo, W.H., Koizumi, H. (2002). "Effects of rainfall events on soil CO_2 flux in a cool temperate deciduous broad-leaved forest." *Ecological Research*. 17: 401-409.

LI-COR Biosciences. Automated Soil CO_2 Flux System & LI-8150 Multiplexer Instruction Manual. (2010).

Liu, X., Guo, Y., Hu, H., Sun, C., Zhao, X., Wei, C. (2015). "Dynamics and controls of CO_2 and CH_4 emissions in the wetland of a montane permafrost region, northeast China." *Atmospheric Environmen*t. 122: 454-462.

Mitsch, W.J., Gosselink, J.G. (2015) Wetlands. 5th Ed. John Wiley & Sons, Inc. Hoboken, New Jersey.

Moore, T.R., Knowles, R. (1989). "The influence of water table levels on methane and carbon dioxide emissions from peatland soils." *Canadian Journal of Soil Science.* 69: 33-38.

National Oceanic & Atmospheric Administration (NOAA). Earth System Research Laboratory (ESRL). Stable and Radiocarbon Isotopes of Carbon Dioxide. http://www.esrl.noaa.gov/gmd/outreach/isotopes/mass_spec.html

National Oceanic & Atmospheric Administration (NOAA). Earth System Research Laboratory (ESRL). Global Monitoring Division. https://www.esrl.noaa.gov/gmd/ccgg/trends/weekly.html

Oertel, C., Matschullat, J., Zurba, K., Zimmermann, F., Erasmi, S. (2016). "Greenhouse gas emission from soils—A review." *Chemi der Erde – Geochemistry*. 76(3): 327-352.

Pataki, D.E., Ehleringer, J.R., Flanagan, L.B., Yakir, D. Bowling, D.R., Still, C.J., Buchman, N., Kaplan, J.O., Berry, J.A. (2003). "The application and interpretation of Keeling plots in terrestrial carbon cycle research." *Global Biogeochemical Cycles*. 17, 1.

Picarro. Cavity Ring-Down Spectroscopy (CRDS). (2016). http://www.picarro.com/technology/cavity_ring_down_spectroscopy.

Reinartz, J.A. (1985) "A Guide to the Natural History of the Cedarburg Bog." University of Wisconsin-Milwaukee. Field Station Bulletin: 18(2).

Rosenberry, D.O., Glaser, P.H., Siegel, D.I. (2006). "The hydrology of northern peatlands as affected by biogenic gas: current developments and research needs." *Hydrological Processes.* 20(17): 3601-3610.

Sharp, Zachary. (2007). 1st Edition. Principles of stable isotopes geochemistry. Pearson Education, Inc. Upper Saddle River, New Jersey.

Sherwood, L, Klandorf, H., Yancey, P. (2013). "Animal Physiology: From Genes to Organisms." 2nd Edition. Brooks/Cole. Belmont, CA.

Silvola, J., Alm, J., Ahlholm, U., Nykänen, H., Martikainen, P.J. (1996). "The contribution of plant roots to CO_2 fluxes from organic soils." *Biology and Fertility of Soils*. 23(2): 126-131.

Solinst Levelogger. User Guide (2015). http://www.solinst.com/products/dataloggers-and-telemetry/3001-levelogger-series/operating-instructions/user-guide/3001-user-guide.pdf.

ThetaProbe ML2x User Manual. http://upgmbh.com/fileadmin/produkte/support/ML2x_Theta_ProbeUserManual_v1.21.pdf.

Tokida, T., Miyazaki, T., Mizoguchi, M. (2005). "Ebullition of methane from peat with falling atmospheric pressure." *Geophysical Research Letters.* 32(13): L13823.

Tokida, T., Miyazaki, T., Mizoguchi, M., Nagata, O., Takakai, F., Kagemoto, A., Hatano, R. (2007). "Falling atmospheric pressure as a trigger for methane ebullition from peatland." *Global Biogeochemical Cycles.* 21: GB2003.

Waddington, J.M., Harrison, K., Kellner, E., Baird, A.J. (2009). "Effect of atmospheric pressure and temperature on entrapped gas content in peat." *Hydrological Processes.* 23: 2970-2980.

Wisconsin Department of Natural Resources. Geographic Information Systems (GIS). http://dnr.wi.gov/. Accessed March 2015.

Wisconsin Department of Natural Resources. http://dnr.wi.gov/topic/lands/naturalareas/documents/topomaps/map02.pdf.

Wisconsin Geological & Natural History Survey. Quaternary Geology of Ozaukee and Washington Counties, Wisconsin. https://wgnhs.uwex.edu/pubs/000115/.

APPENDIX A: BASIC STATISTICS

Basic statistics of measured variables for the duration of each field season (i.e. average atmospheric temperature for designated period, not for entire year) produced in JMP from LICOR and Weather data in Appendix D.

May 22 – Nov 12, 2014	**Average**	**Std Dev**	**Median**	**Max**	**Min**	**Sample Size**
Soil CO_2 Flux (mg/min-m^2)	6.41	14.49	3.34	530.04	0.02	4832
Cumulative Soil CO_2 Flux = 814,565.80 mg/m^2 ~ 0.815 kg/m^2						
Surface CO_2 Concentration (ppm)	442.93	88.83	403.31	857.07	336.59	4832
Radiation (kW/m^2)	0.20	0.28	0.02	1	0	8328
Wind Speed (m/s)	1.13	1.01	0.98	5.4	0	8328
Atmospheric Pressure (kPa)	101.58	0.59	101.63	103.12	99.81	8193
Atmospheric Temperature (°C)	15.54	6.82	15.98	31.74	-6.71	8328
Soil Temperature (°C)	13.95	3.81	14.68	19.52	5.68	4832
Precipitation (mm)	0.05	0.49	0	14.10	0	8400
Cumulative Precipitation = 461.89 mm						
Jun 1 – Oct 28, 2015	**Average**	**Std Dev**	**Median**	**Max**	**Min**	**Sample Size**
Soil CO_2 Flux (mg/min-m^2)	6.62	20.09	3.45	676.47	0.00	2862
Cumulative Soil CO_2 Flux = 1,100,242.92 mg/m^2 ~ 1.100 kg/m^2						
Surface CO_2 Concentration (ppm)	459.70	118.36	407.06	1059.78	349.27	2862
Radiation (kW/m^2)	0.22	0.29	0.04	1	0	7200
Wind Speed (m/s)	1.15	1.07	0.02	5.25	0	7200
Atmospheric Pressure (kPa)	101.61	0.59	101.61	103.18	99.25	7200
Atmospheric Temperature (°C)	17.56	6.03	17.65	32.13	-3.16	7200
Soil Temperature (°C)	16.97	1.80	17.3	20.15	10.32	2289
Soil Moisture Content	0.61	0.02	0.62	0.681	0.012	2858
Precipitation (mm)	0.06	0.57	0	31.63	0	7200
Cumulative Precipitation = 398.57 mm						

APPENDIX B: JMP STATISTICAL CORRELATIONS

Multiple linear regression model parameters and results (alpha = 0.2) produced in JMP using LICOR and Weather data from Appendix D.

Dependent Variable	Range	Independent Variable(s) & p value(s)	R Square
Soil CO_2 Flux	All	Atm. Temperature (<0.0001) Wind Speed (<0.0001) Soil Temperature (<0.0001) Atm. Pressure (<0.0001) Surface CO_2 Concentration (0.0037)	0.046899
Soil CO_2 Flux	Day	Atm. Temperature (<0.0001) Wind Speed (<0.0001) Soil Temperature (0.0044)	0.030961
Soil CO_2 Flux	Night	Atm. Temperature (<0.0001) Soil Temperature (<0.0001) Wind Speed (<0.0001) Surface CO_2 Concentration (0.0167)	0.073316
Soil CO_2 Flux	< 5 mg/min-m^2	Soil Temperature (<0.0001) Atm. Temperature (<0.0001) Atm. Pressure (<0.0001) Surface CO_2 Concentration (<0.0001) Radiation (0.0011) Soil Moisture Content (0.0082) Wind Speed (0.0159)	0.19136
Soil CO_2 Flux	< 5 mg/min-m^2	Soil Temperature (<0.0001)	0.276164
Soil CO_2 Flux	< 5 mg/min-m^2 (Day)	Soil Temperature (<0.0001) Soil Moisture Content (<0.0001) Wind Speed (<0.0001)	0.132718
Soil CO_2 Flux	< 5 mg/min-m^2 (Night)	Soil Temperature (<0.0001) Atm. Pressure (<0.0001) Wind Speed (0.0032)	0.385887
Soil CO_2 Flux	< 5 mg/min-m^2 (Night)	Soil Temperature (<0.0001)	0.416979
Soil CO_2 Flux	5 – 50 mg/min-m^2	Wind Speed (<0.0001) Surface CO_2 Concentration (<0.0001) Atm. Temperature (0.0011) Precipitation (0.0304)	0.023383
Soil CO_2 Flux	5 – 50 mg/min-m^2 (Day)	Wind Speed (<0.0001)	0.016758
Soil CO_2 Flux	5 – 50 mg/min-m^2 (Night)	Soil Temperature (<0.0001) Atm. Temperature (<0.0001)	0.225924
Soil CO_2 Flux	>50 mg/min-m^2	Soil Temperature (0.0149) Radiation (0.0193)	0.087588
Soil CO_2 Flux	>50 mg/min-m^2 (Day)	None	N/A
Soil CO_2 Flux	>50 mg/min-m^2 (Night)	None	N/A
Dependent Variable	**Range**	**Independent Variable(s) & p value(s)**	**R Square**
Surface CO_2 Concentration	All	Wind Speed (<0.0001) Soil Temperature (<0.0001) Atm. Temperature (0.0001) Radiation (0.0018) Soil Moisture Content (0.0403)	0.307727
Surface CO_2 Concentration	Day	Wind Speed (<0.0001) Atm. Temperature (<0.0001) Soil Temperature (<0.0001)	0.227855
Surface CO_2 Concentration	Night	Wind Speed (<0.0001)	0.296597

		Soil Temperature (<0.0001)	
Surface CO_2 Concentration	< 425 ppm	Radiation (<0.0001) Atm. Temperature (<0.0001) Wind Speed (0.0002)	0.142406
Surface CO_2 Concentration	< 400 ppm (Day)	Atm. Temperature (<0.0001) Radiation (<0.0001) Wind Speed (<0.0001)	0.095618
Surface CO_2 Concentration	< 400 ppm (Night)	Wind Speed (<0.0001) Atm. Temperature (<0.0001) Soil Temperature (0.0003)	0.129578
Surface CO_2 Concentration	>400 ppm	Wind Speed (<0.0001) Soil Temperature (<0.0001)	0.226263
Surface CO_2 Concentration	>400 ppm (Day)	Wind Speed (<0.0001) Soil Temperature (<0.0001) Atm. Temperature (<0.0001)	0.258038
Surface CO_2 Concentration	>400 ppm (Night)	Wind Speed (<0.0001) Soil Temperature (<0.0001)	0.20024
Surface CO_2 Concentration	Wind Speed < 2 m/s	Wind Speed (<0.0001) Soil Temperature (<0.0001) Atm. Temperature (<0.0001) Radiation (0.0004)	34.0145
Surface CO_2 Concentration	Wind Speed < 1.5 m/s	Wind Speed (<0.0001) Soil Temperature (<0.0001) Atm. Temperature (<0.0001)	0.307192
Surface CO_2 Concentration	Wind Speed < 1 m/s	Wind Speed (<0.0001) Soil Temperature (<0.0001) Atm. Temperature (<0.0001) Radiation (0.0117)	0.228998
Surface CO_2 Concentration	Wind Speed >1 m/s	Radiation (<0.0001) Atm. Temperature (<0.0001)	0.069504
Surface CO_2 Concentration	Wind Speed >2 m/s	Radiation (<0.0001) Precipitation (<0.0001) Atm. Temperature (0.0001) Wind Speed (0.0025)	0.037272
Surface CO_2 Concentration	Wind Speed >2 m/s (Day)	Precipitation (0.0012) Wind Speed (0.0036) Radiation (0.0053) Atm. Temperature (0.0255)	0.023448
Surface CO_2 Concentration	Wind Speed >2 m/s (Night)	Atm. Temperature (<0.0001) Precipitation (<0.001)	0.365798

APPENDIX C: COMPLETE LICOR AND WEATHER PLOTS

Complete timeline of collected LICOR and Weather Station data, including soil CO_2 flux (pink bars), radiation (purple line), wind speed (green line), surface CO_2 concentration (light blue line), atmospheric temperature (orange line), precipitation (blue triangles), atmospheric pressure (black line), soil temperature (red line), and volumetric soil moisture content (dark blue line). Produced in Grapher using LICOR and Weather data from Appendix D.

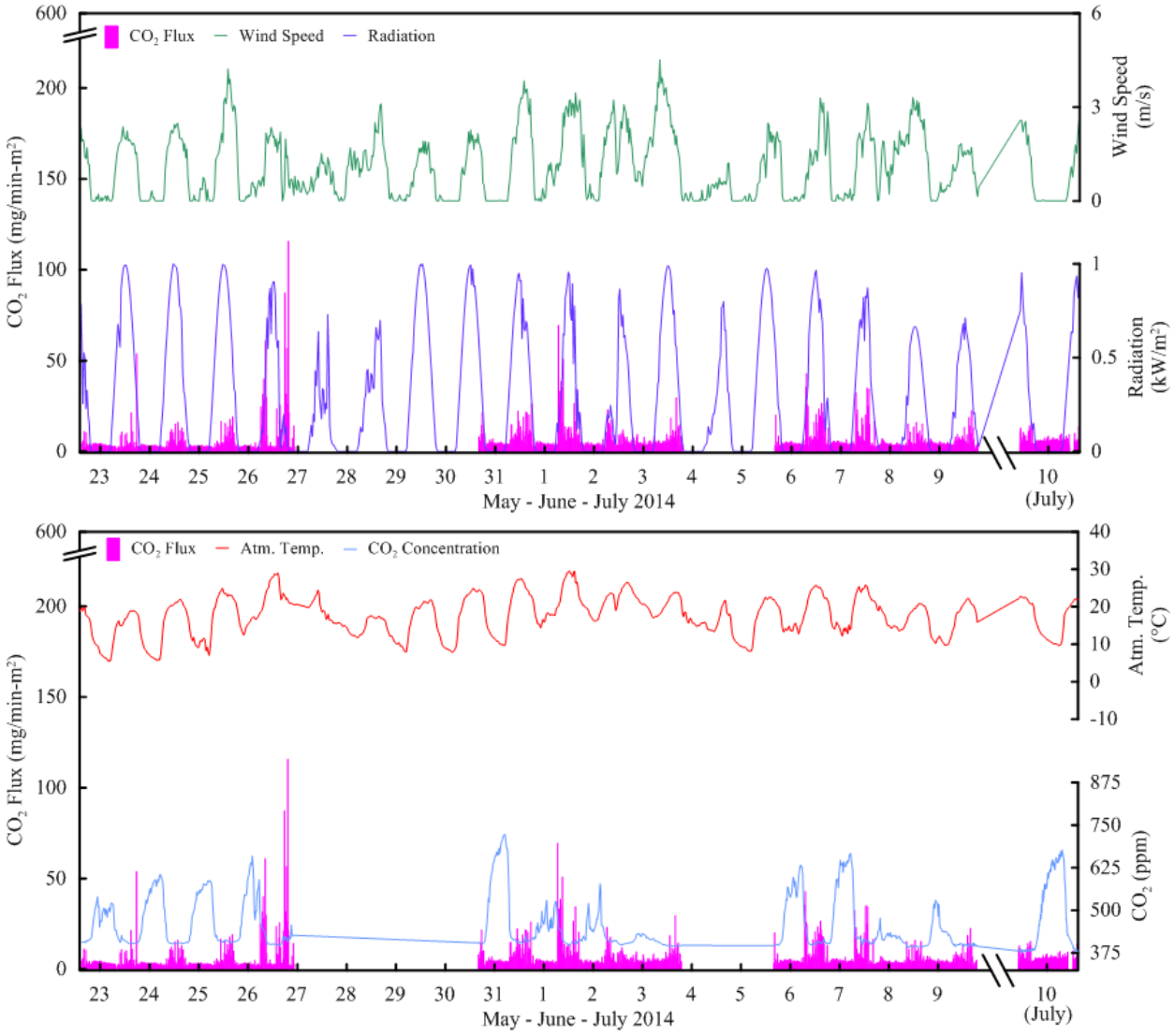

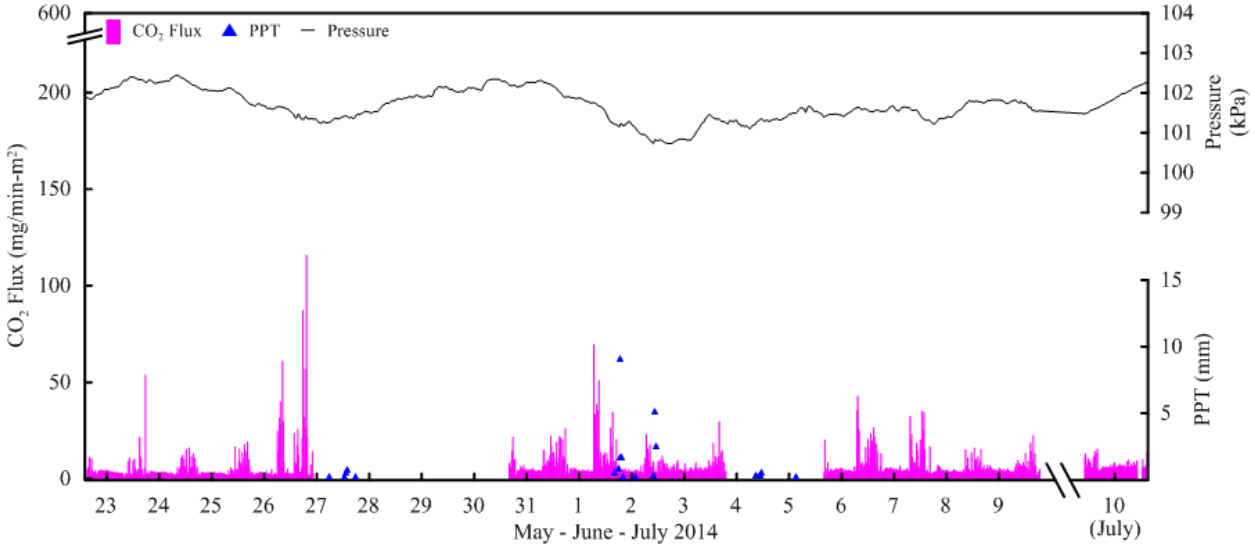
CO2 Flux
PPT
Pressure
CO2 Flux (mg/min-m2)
Pressure (kPa)
PPT (mm)
May - June - July 2014
(July)

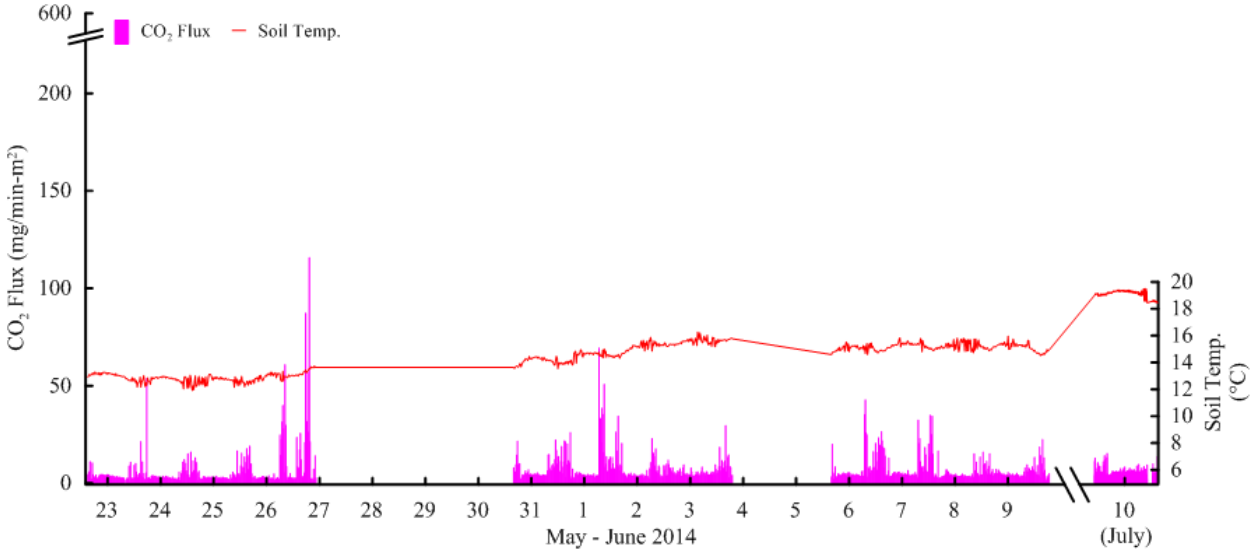
CO2 Flux
Soil Temp.
CO2 Flux (mg/min-m2)
Soil Temp. (°C)
May - June 2014
(July)

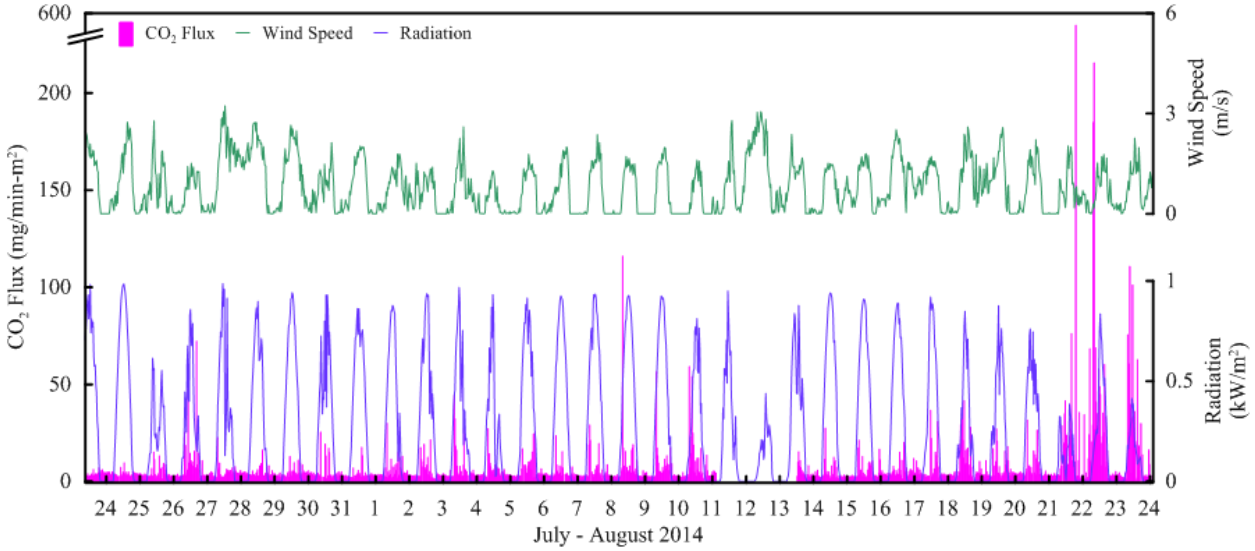
CO2 Flux
Wind Speed
Radiation
CO2 Flux (mg/min-m2)
Wind Speed (m/s)
Radiation (kW/m2)
July - August 2014

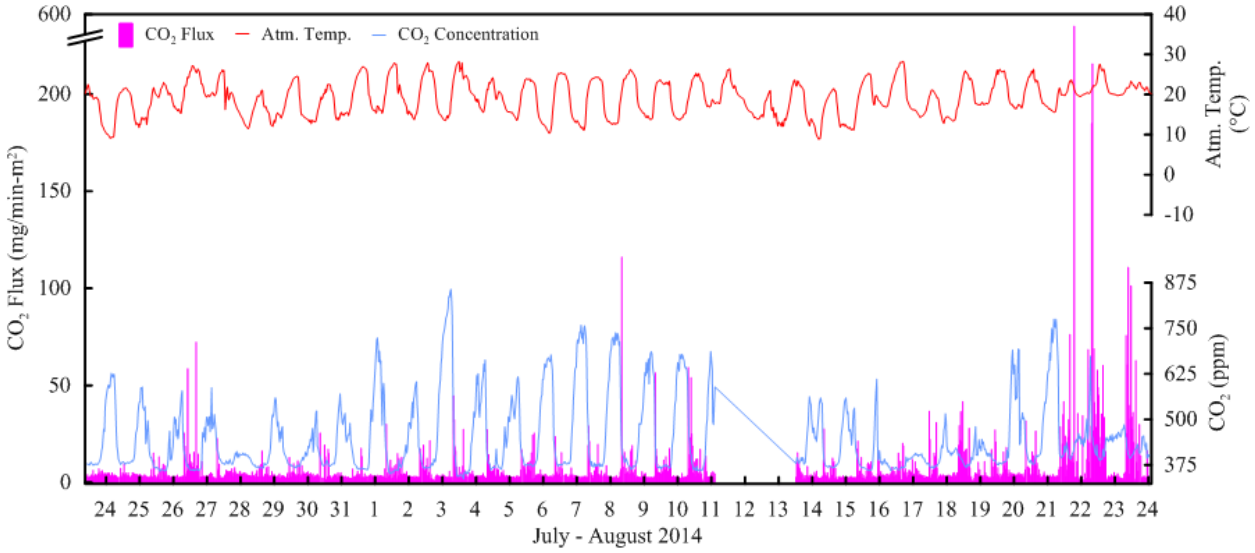
CO2 Flux
Atm. Temp.
CO2 Concentration
CO2 Flux (mg/min-m2)
Atm. Temp. (°C)
CO2 (ppm)
July - August 2014

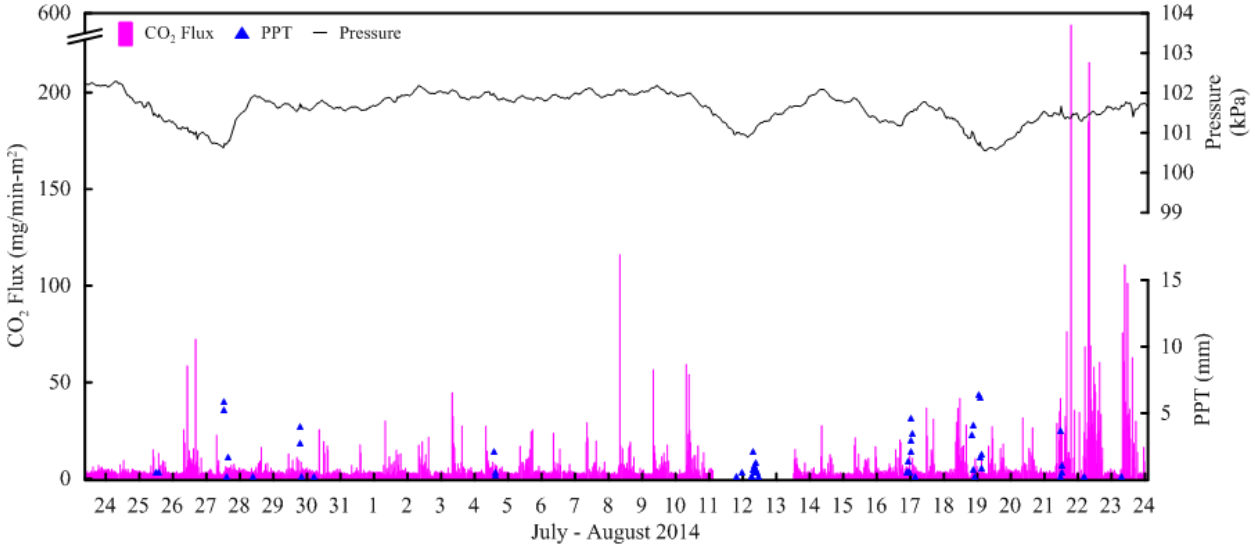
CO2 Flux
PPT
Pressure
CO2 Flux (mg/min-m2)
Pressure (kPa)
PPT (mm)
July - August 2014

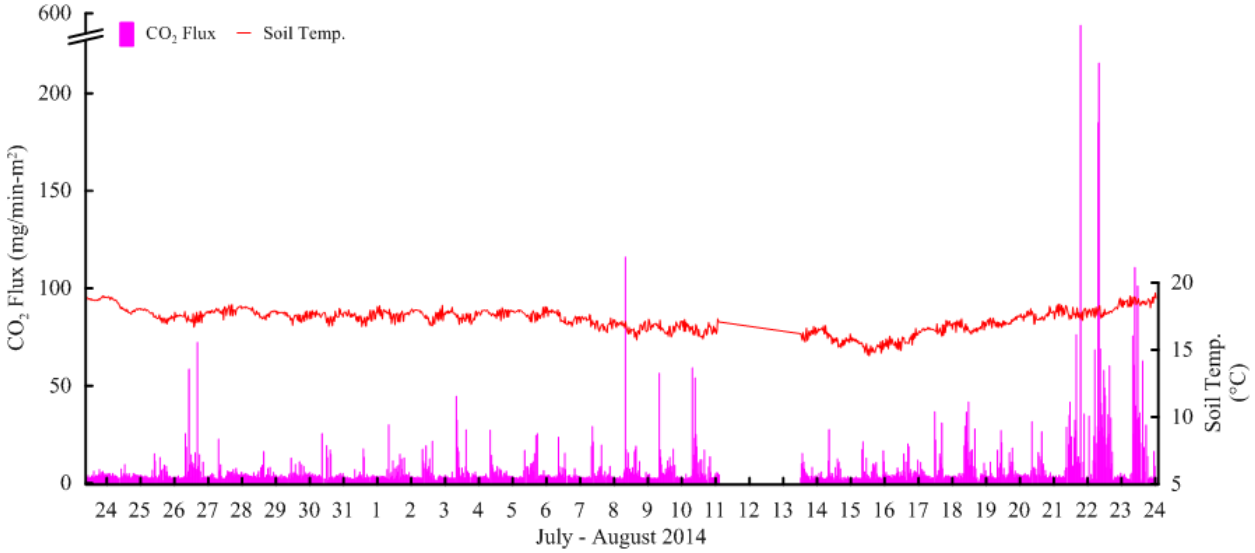
CO2 Flux
Soil Temp.
CO2 Flux (mg/min-m2)
Soil Temp. (°C)
July - August 2014

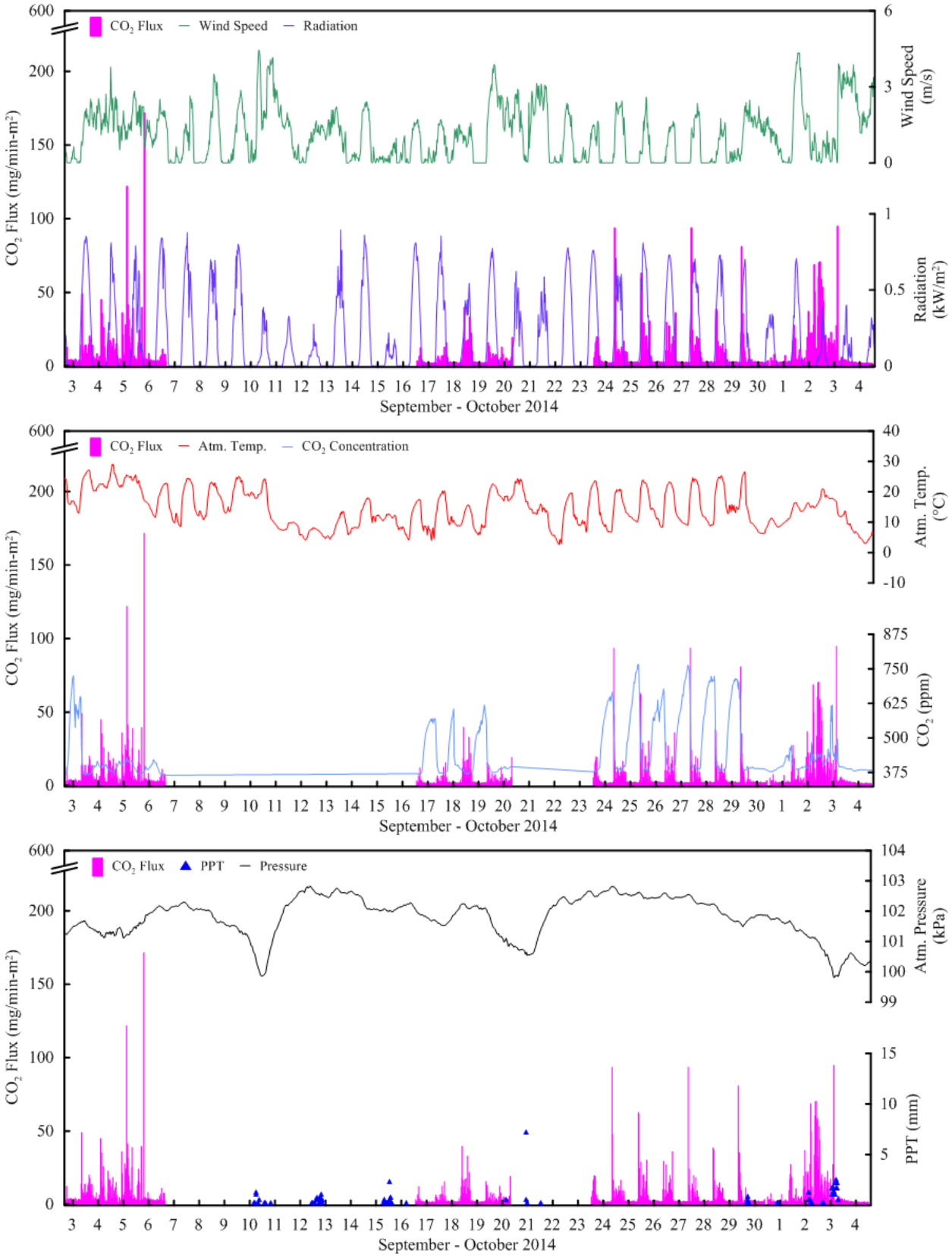
CO2 Flux
Wind Speed
Radiation
CO2 Flux (mg/min-m2)
Wind Speed (m/s)
Radiation (kW/m2)
September - October 2014
CO2 Flux
Atm. Temp.
CO2 Concentration
Atm. Temp. (°C)
CO2 (ppm)
September - October 2014
CO2 Flux
PPT
Pressure
Atm. Pressure (kPa)
PPT (mm)
September - October 2014

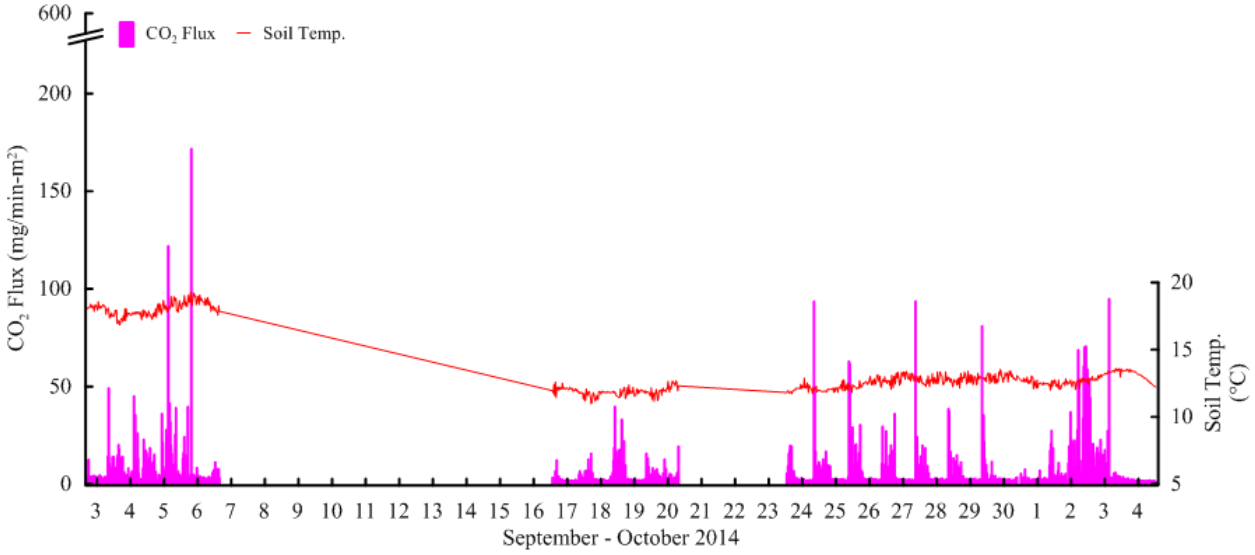
CO2 Flux
Soil Temp.
CO2 Flux (mg/min-m2)
Soil Temp. (°C)
September - October 2014

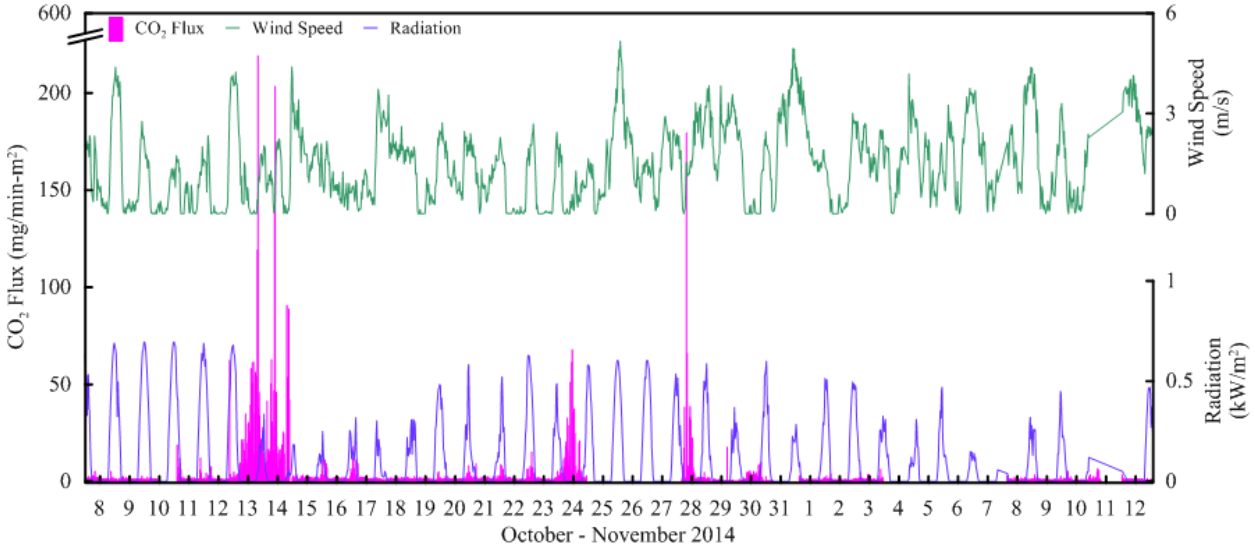
CO2 Flux
Wind Speed
Radiation
CO2 Flux (mg/min-m2)
Wind Speed (m/s)
Radiation (kW/m2)
October - November 2014

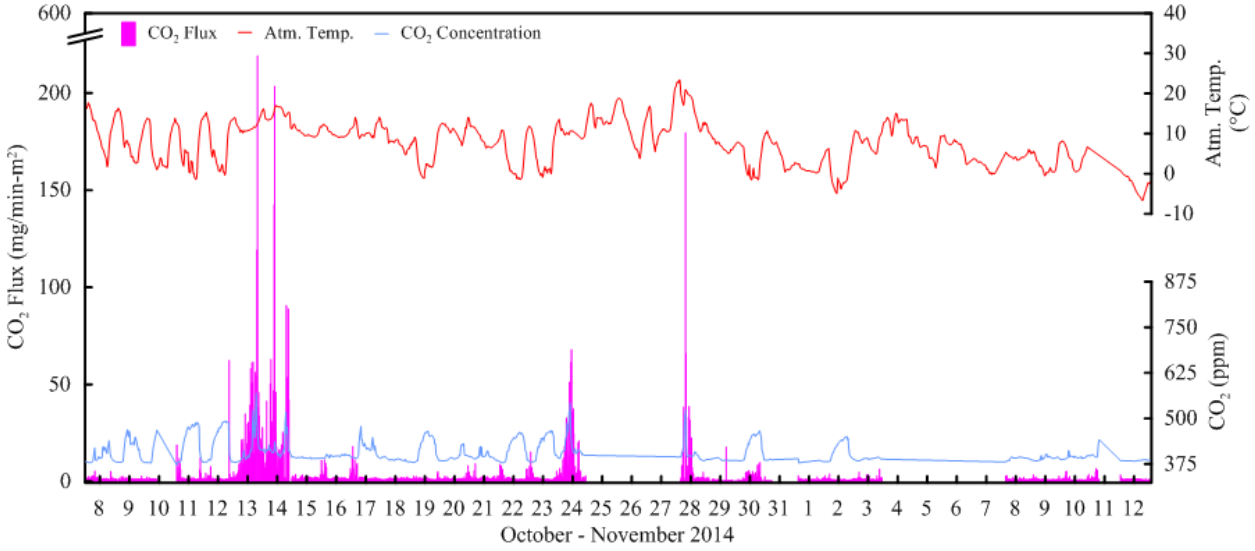
CO2 Flux
Atm. Temp.
CO2 Concentration
CO2 Flux (mg/min-m2)
Atm. Temp. (°C)
CO2 (ppm)
October - November 2014

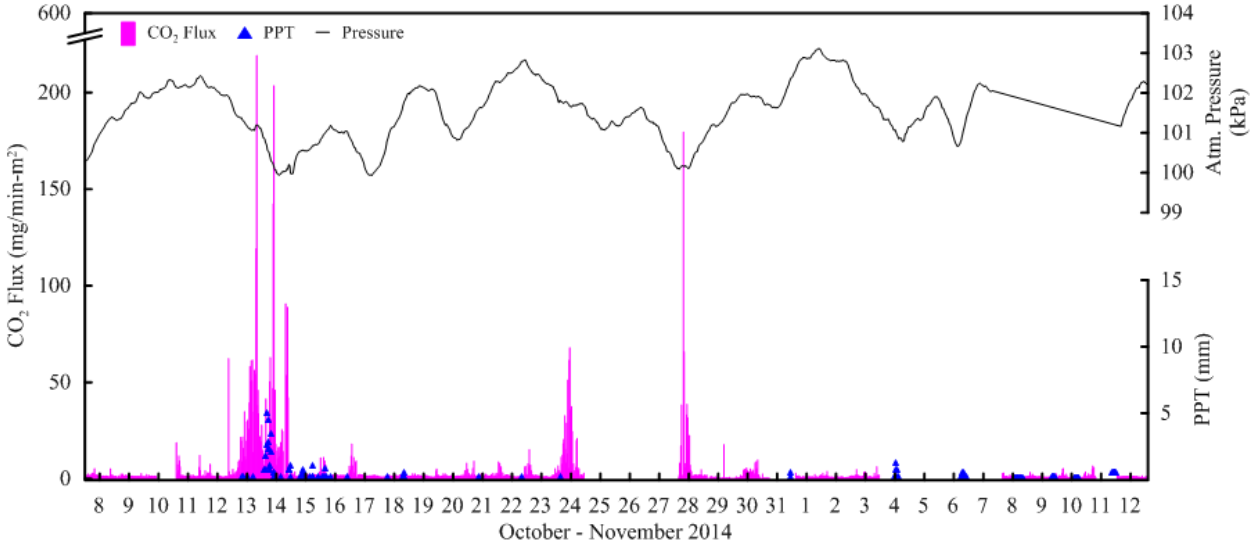
CO2 Flux
PPT
Pressure
CO2 Flux (mg/min-m2)
Atm. Pressure (kPa)
PPT (mm)
October - November 2014

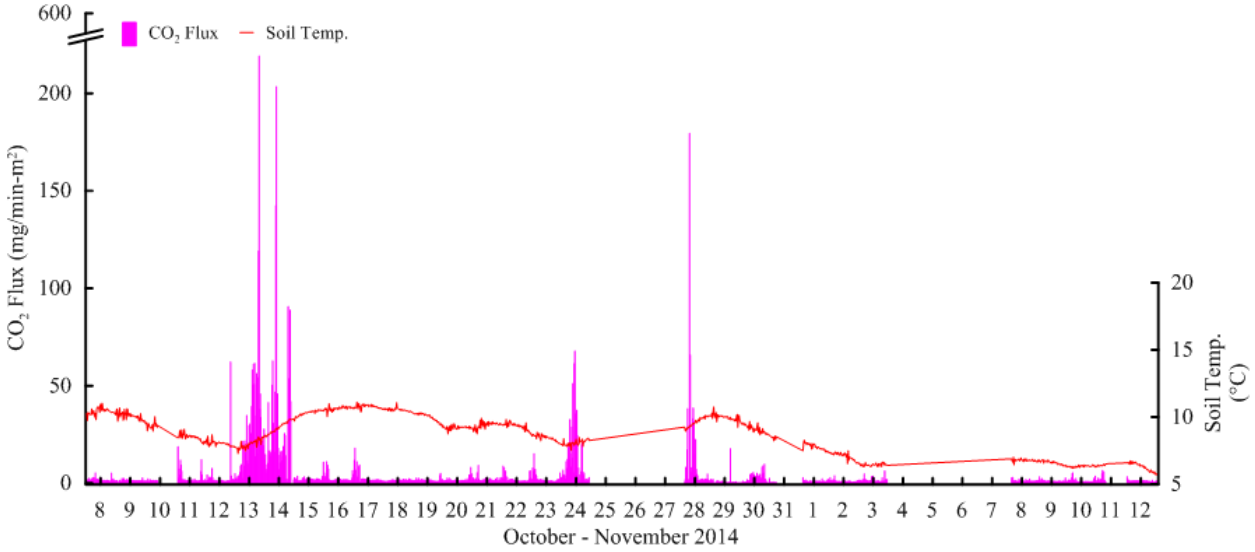
CO2 Flux
Soil Temp.
CO2 Flux (mg/min-m2)
Soil Temp. (°C)
October - November 2014

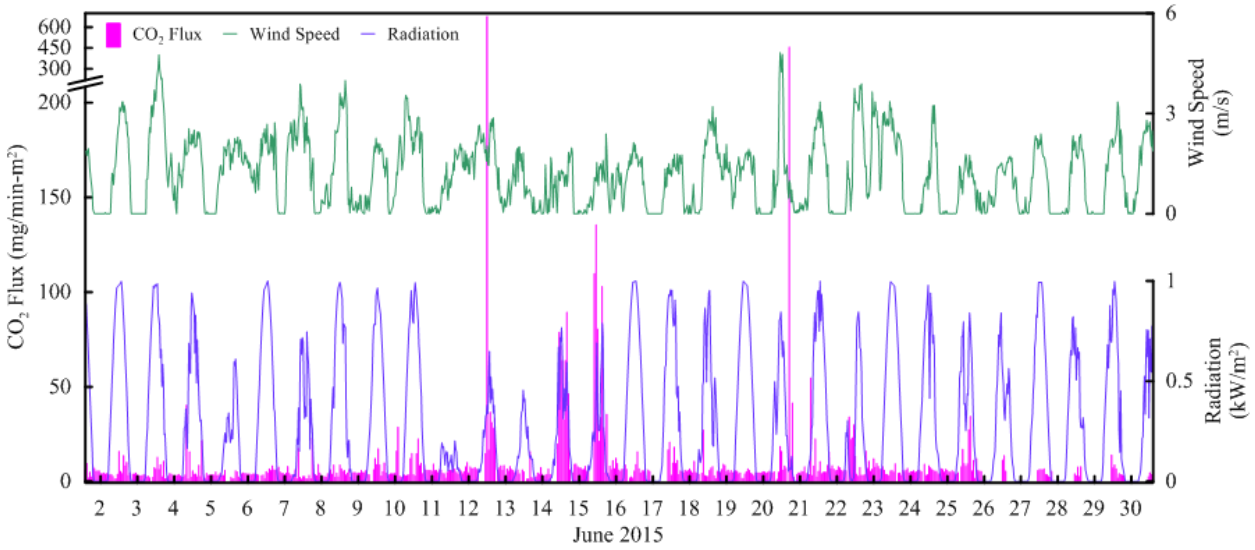
CO2 Flux
Wind Speed
Radiation
CO2 Flux (mg/min-m2)
Wind Speed (m/s)
Radiation (kW/m2)
June 2015

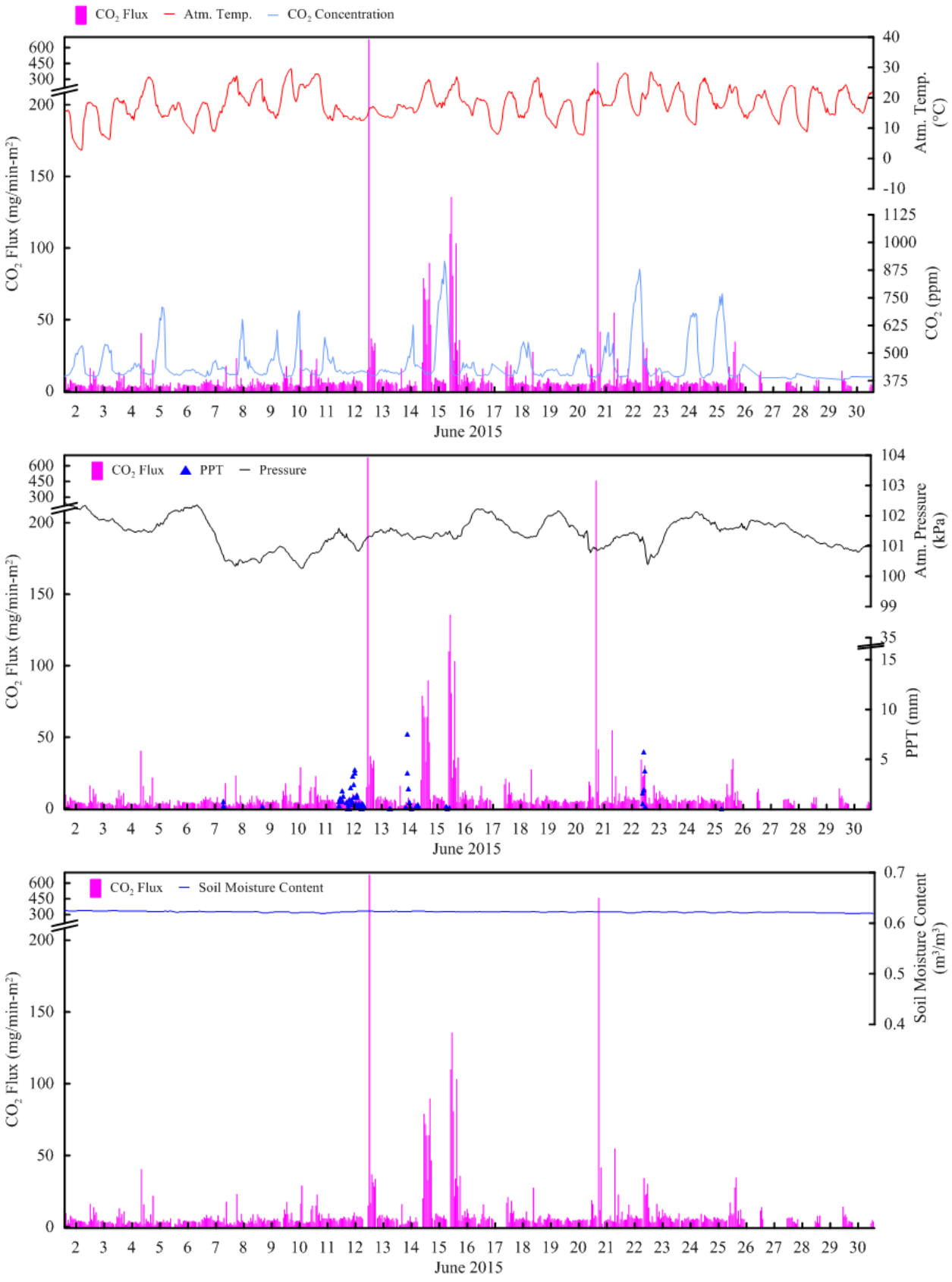
CO2 Flux
Atm. Temp.
CO2 Concentration
CO2 Flux (mg/min-m2)
Atm. Temp. (°C)
CO2 (ppm)
June 2015
CO2 Flux
PPT
Pressure
CO2 Flux (mg/min-m2)
Atm. Pressure (kPa)
PPT (mm)
June 2015
CO2 Flux
Soil Moisture Content
CO2 Flux (mg/min-m2)
Soil Moisture Content (m3/m3)
June 2015

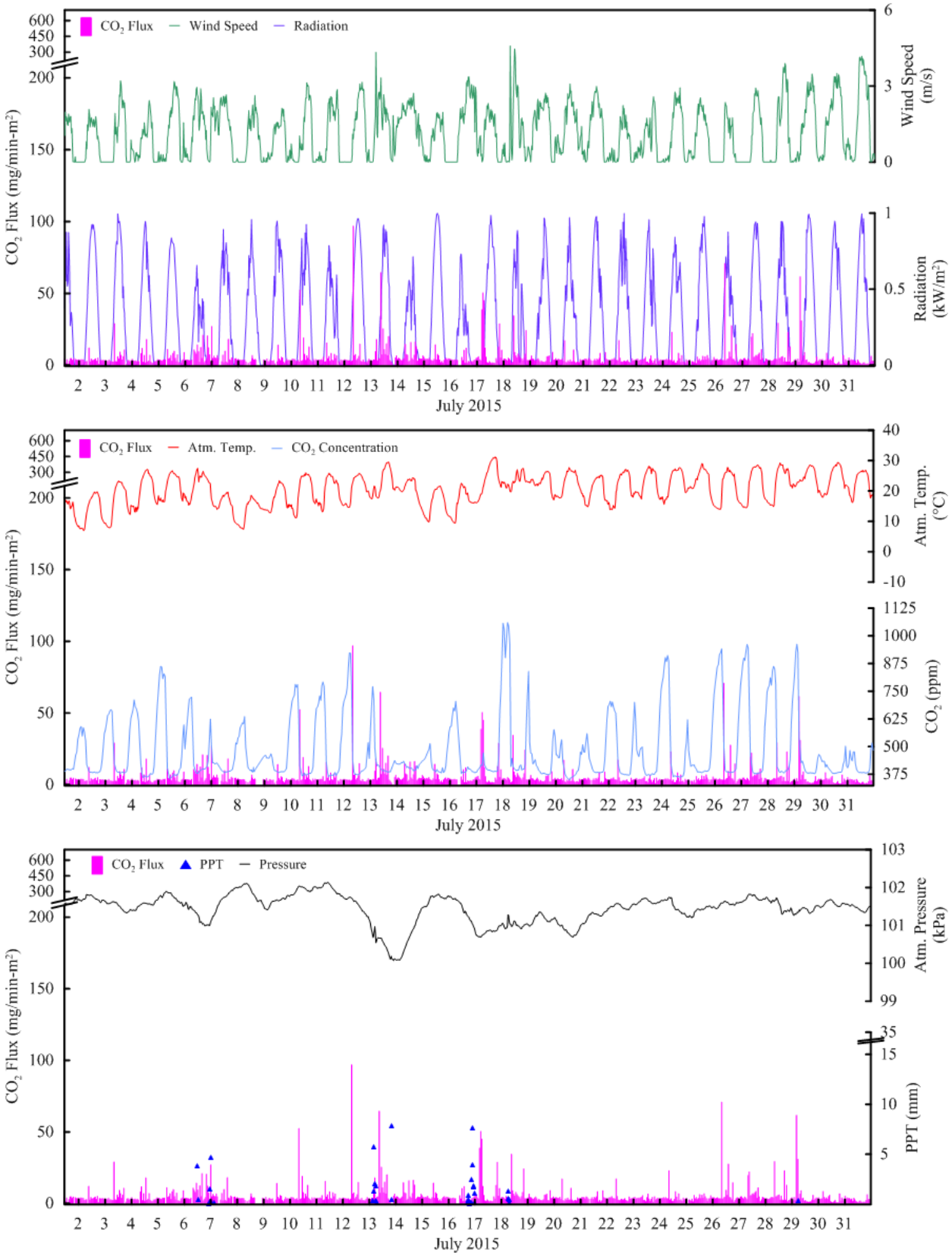
CO2 Flux
Wind Speed
Radiation
CO2 Flux (mg/min-m2)
Wind Speed (m/s)
Radiation (kW/m2)
July 2015
CO2 Flux
Atm. Temp.
CO2 Concentration
Atm. Temp. (°C)
CO2 (ppm)
July 2015
CO2 Flux
PPT
Pressure
Atm. Pressure (kPa)
PPT (mm)
July 2015

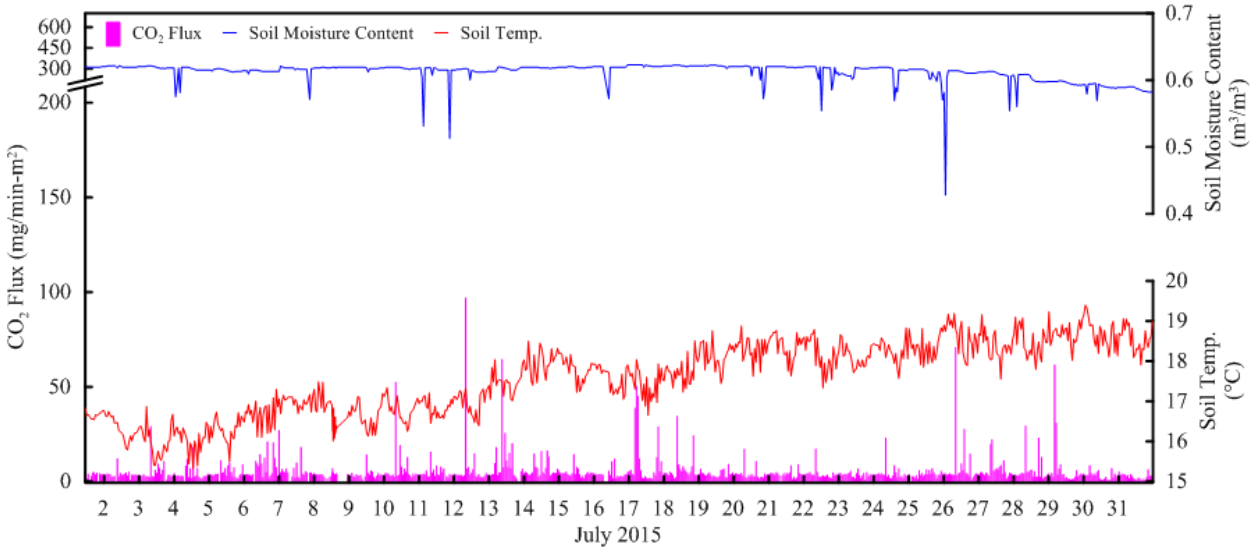
CO2 Flux
Soil Moisture Content
Soil Temp.
CO2 Flux (mg/min-m2)
Soil Moisture Content (m3/m3)
Soil Temp. (°C)
July 2015

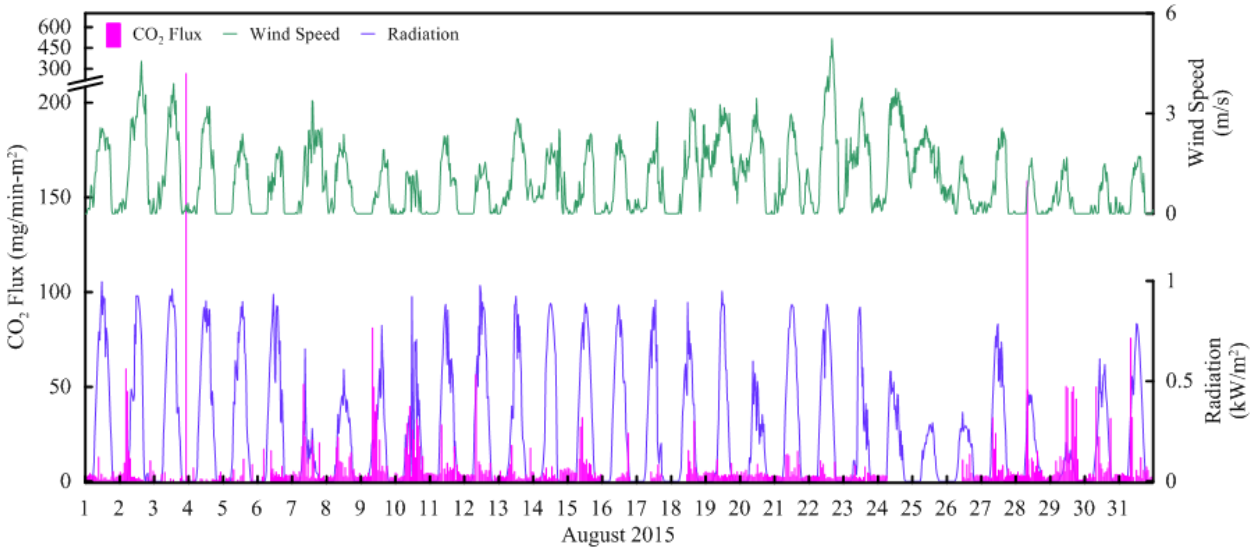
CO2 Flux
Wind Speed
Radiation
CO2 Flux (mg/min-m2)
Wind Speed (m/s)
Radiation (kW/m2)
August 2015

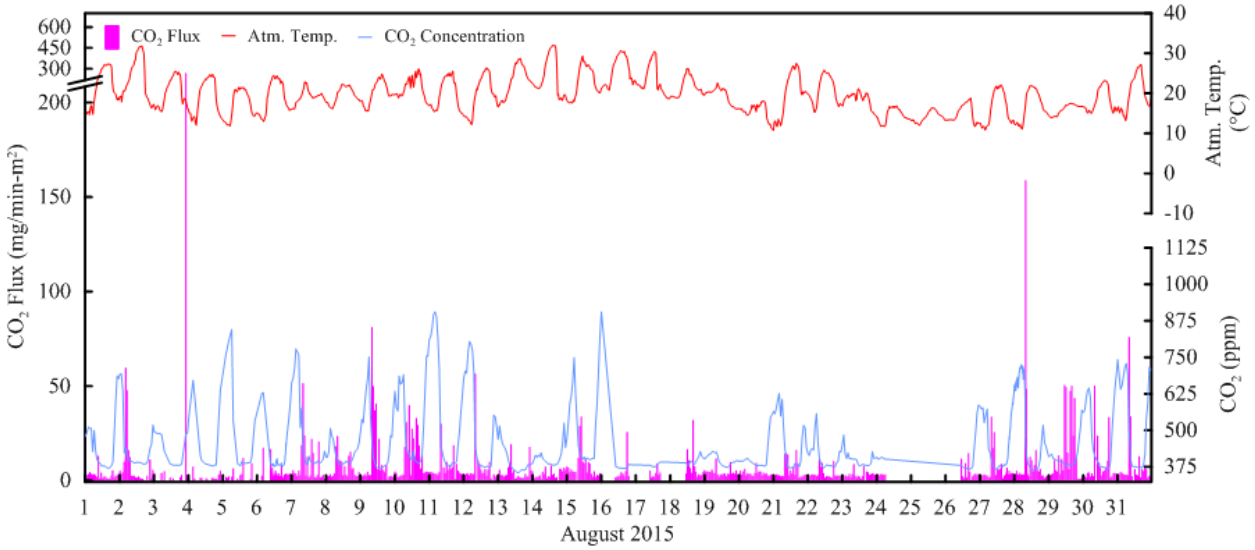
CO2 Flux
Atm. Temp.
CO2 Concentration
CO2 Flux (mg/min-m2)
Atm. Temp. (°C)
CO2 (ppm)
August 2015

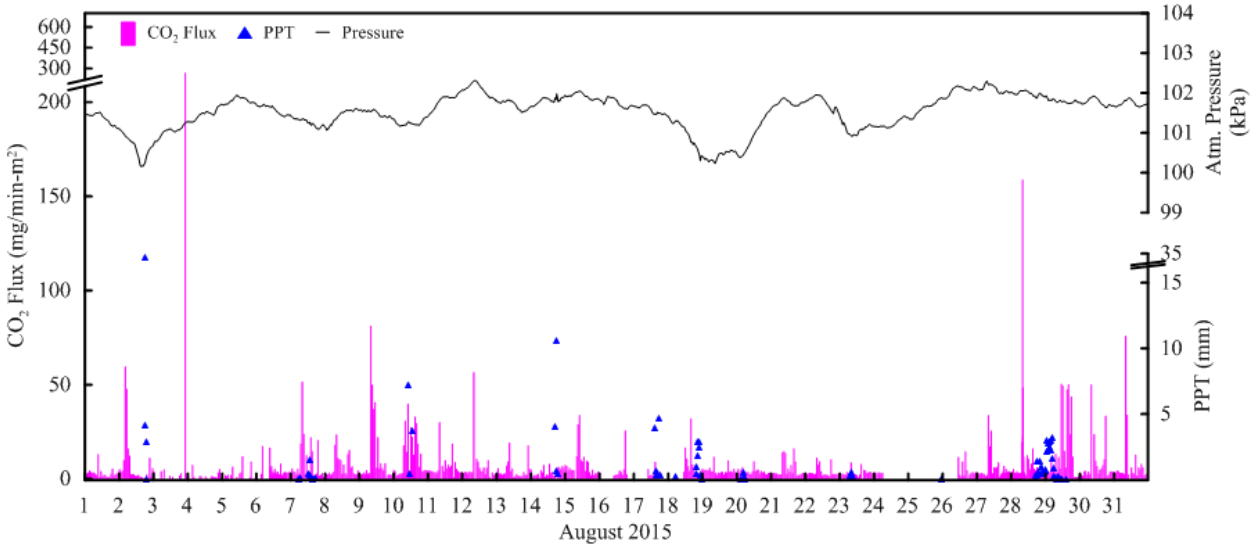
CO2 Flux
PPT
Pressure
CO2 Flux (mg/min-m2)
Atm. Pressure (kPa)
PPT (mm)
August 2015

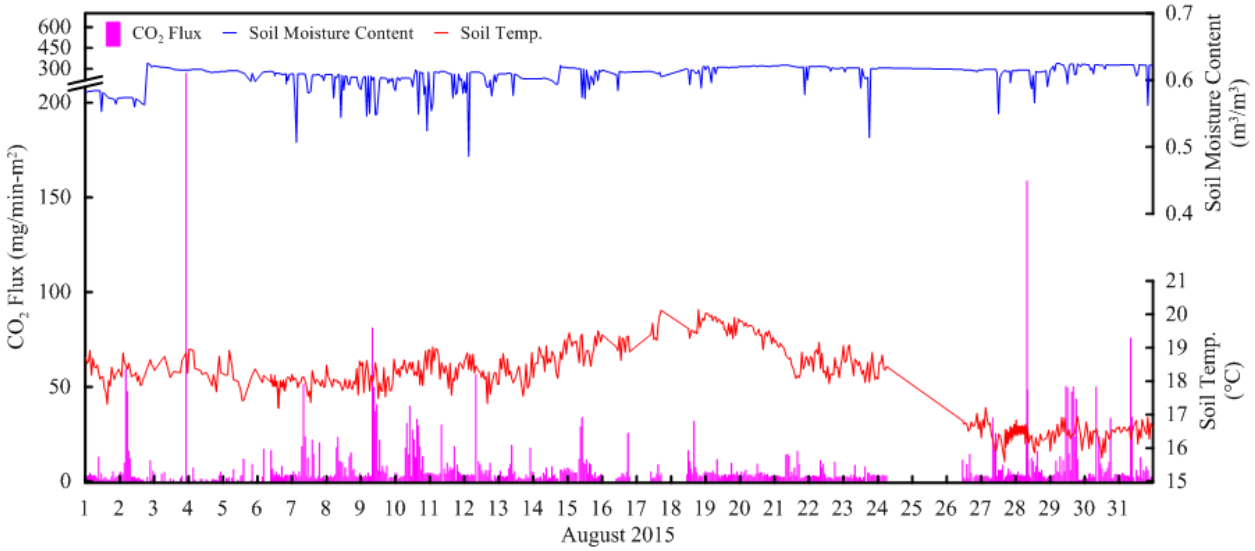
CO2 Flux
Soil Moisture Content
Soil Temp.
CO2 Flux (mg/min-m2)
Soil Moisture Content (m3/m3)
Soil Temp. (°C)
August 2015

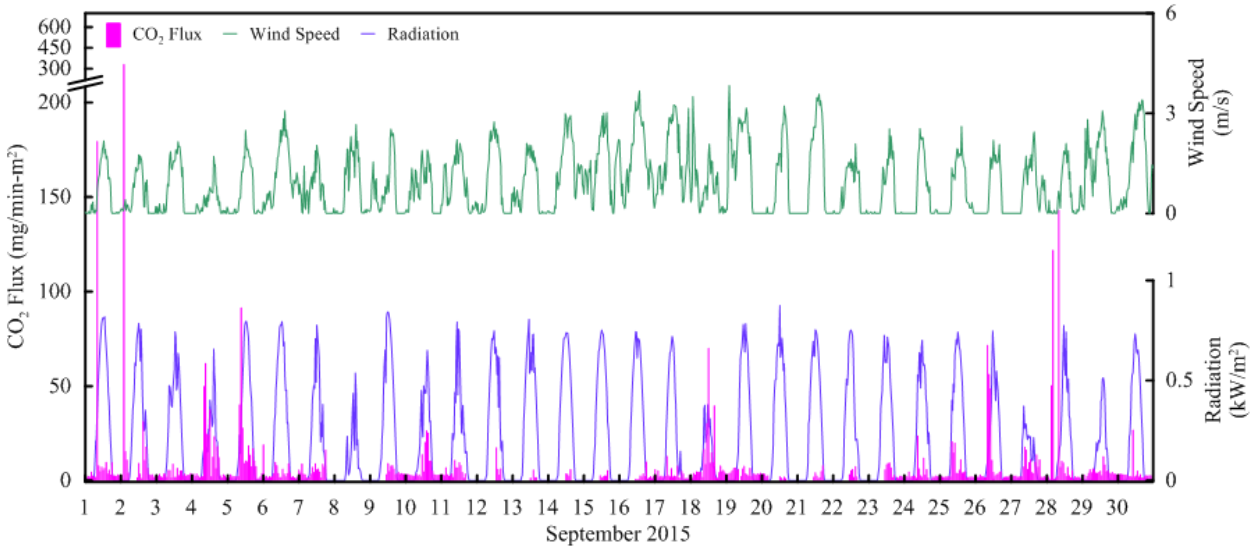
CO2 Flux
Wind Speed
Radiation
CO2 Flux (mg/min-m2)
Wind Speed (m/s)
Radiation (kW/m2)
September 2015

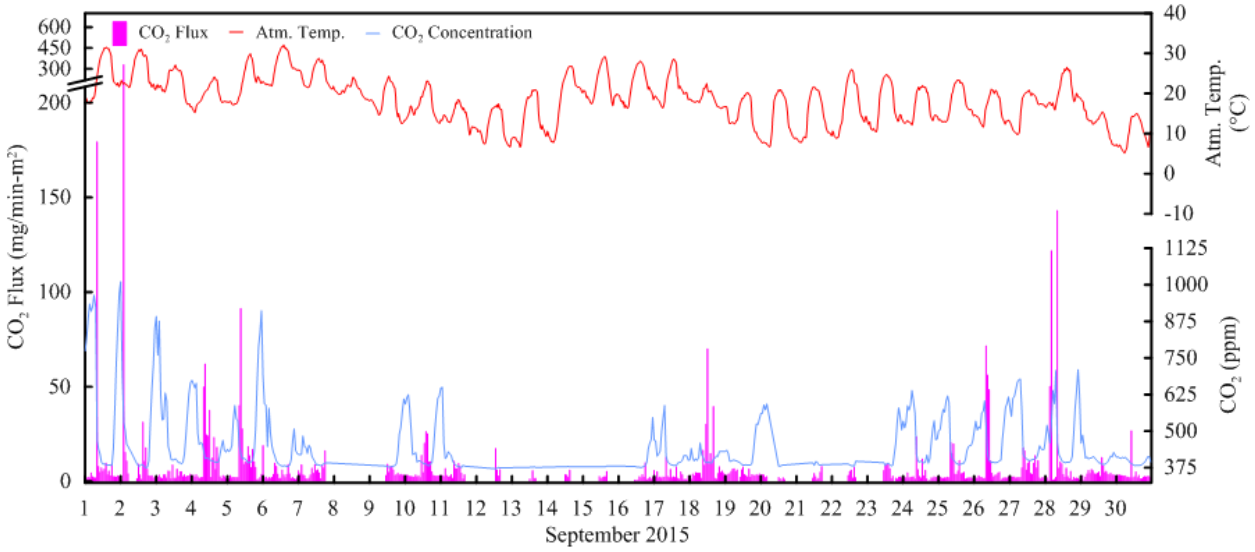
CO2 Flux
Atm. Temp.
CO2 Concentration
CO2 Flux (mg/min-m2)
Atm. Temp. (°C)
CO2 (ppm)
September 2015

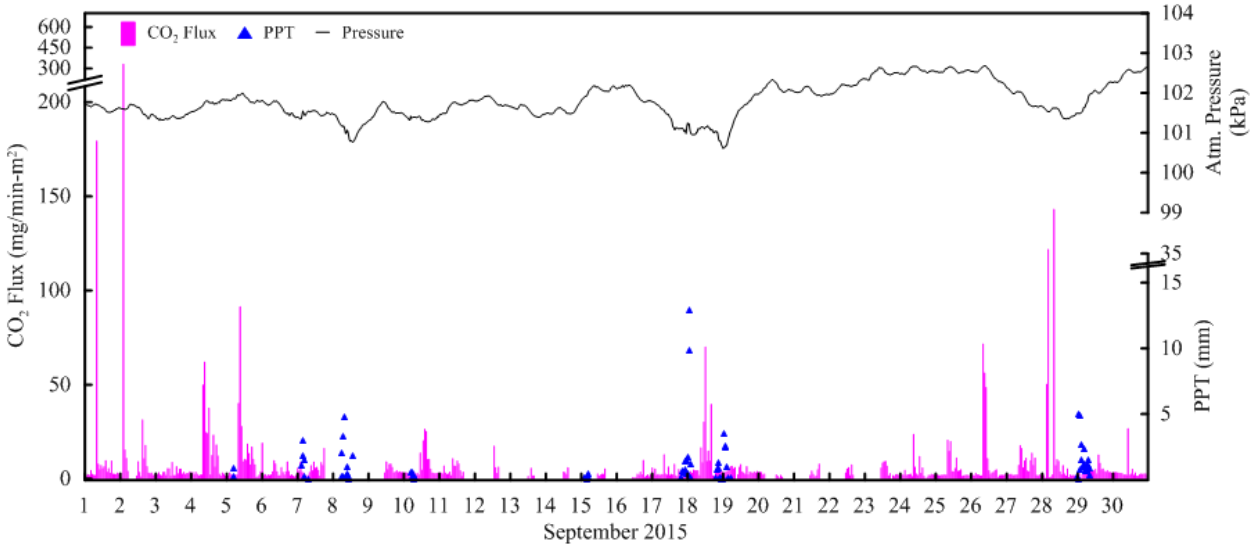
CO2 Flux
PPT
Pressure
CO2 Flux (mg/min-m2)
Atm. Pressure (kPa)
PPT (mm)
September 2015

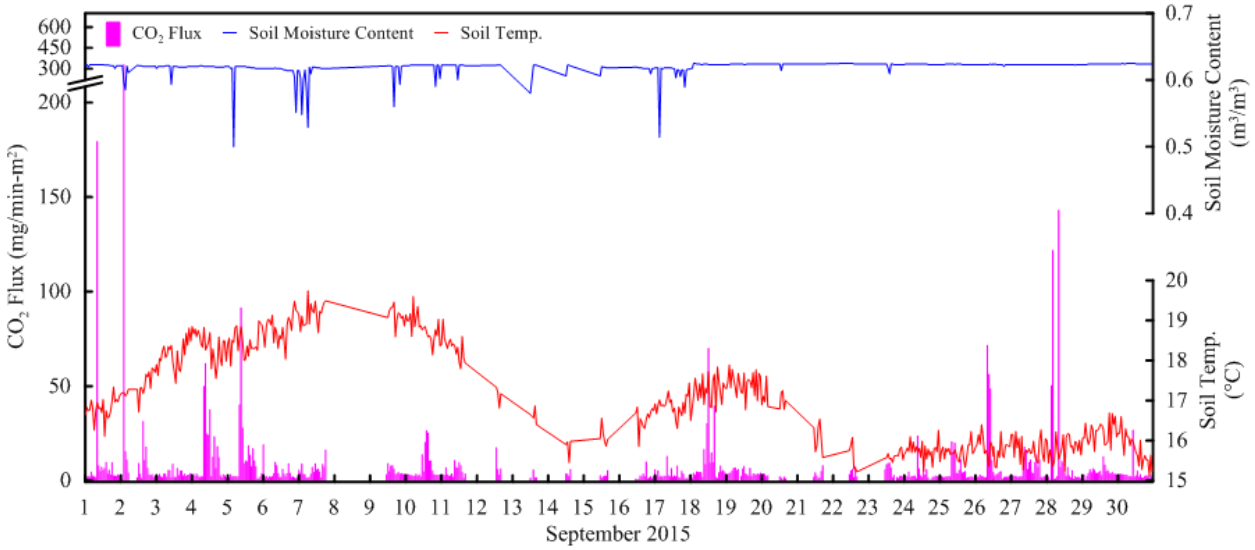
CO2 Flux
Soil Moisture Content
Soil Temp.
CO2 Flux (mg/min-m2)
Soil Moisture Content (m3/m3)
Soil Temp. (°C)
September 2015

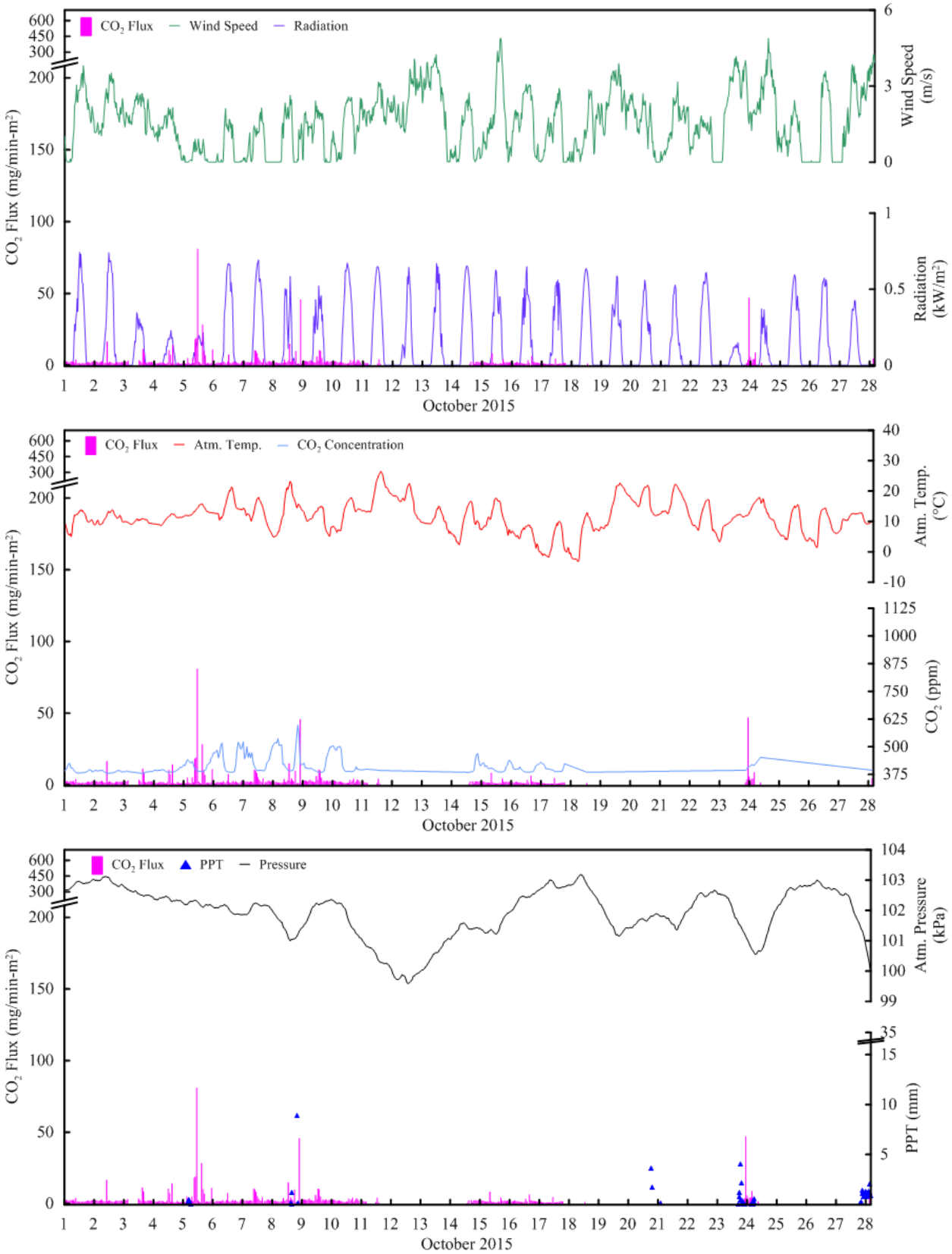
CO2 Flux
Wind Speed
Radiation
CO2 Flux (mg/min-m2)
Wind Speed (m/s)
Radiation (kW/m2)
October 2015
CO2 Flux
Atm. Temp.
CO2 Concentration
Atm. Temp. (°C)
CO2 (ppm)
October 2015
CO2 Flux
PPT
Pressure
Atm. Pressure (kPa)
PPT (mm)
October 2015

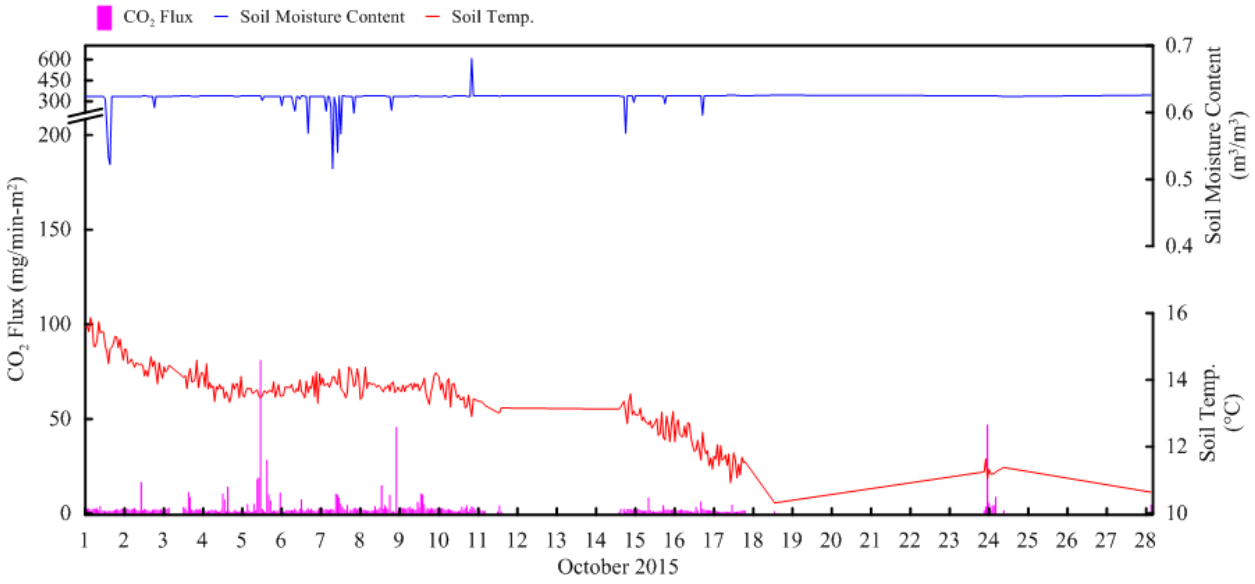
CO2 Flux
Soil Moisture Content
Soil Temp.
600
450
300
200
150
100
50
0
CO2 Flux (mg/min-m2)
0.7
0.6
0.5
0.4
Soil Moisture Content (m3/m3)
16
14
12
10
Soil Temp. (°C)
1 2 3 4 5 6 7 8 9 10 11 12 13 14 15 16 17 18 19 20 21 22 23 24 25 26 27 28
October 2015

APPENDIX D: SUPPLEMENTAL DATA SPREADSHEETS

Appendix D includes complete LICOR, Weather Station, Picarro, and IRMS-EA data sets as an electronic file (Excel spreadsheets) titled "APPENDIX_D_Raw_Data_File.xlsx" outlined in the following table.

Spreadsheet	Description
Filtered_LICOR_and_Weather	Compilation of 2014 and 2015 LICOR and weather station data used in analyses, filtered from raw data according to quality control methods (see section 3.6).
RAW_LICOR_2014	Raw LICOR data collected from 2014 field season (prior to quality control).
RAW_LICOR_2015	Raw LICOR data collected from 2015 field season (prior to quality control).
Weather_2014	Complete set of weather data collected from university Weather Station (see Figure 1b), 2014.
Weather_2015	Complete set of weather data collected from the university Weather Station (see Figure 1b), 2015.
Monitoring_well	Transducer data during 2014, 2015 field seasons collected from Field Site location (see Figure 1b). Note: corrected water level does not reflect actual water table conditions relative to surface (see section 4.6).
Picarro_8July2015	Picarro stable isotope analyzer data collected at Field Site (see Figure 1b) July 8th, 2015 (see sections 3.2, 4.5)
Picarro_6August2015	Picarro stable isotope analyzer data collected at Field Site (see Figure 1b) August 6th, 2015 (see sections 3.2, 4.5)
Picarro_27-28August2015	Picarro stable isotope analyzer data collected at Field Site (see Figure 1b) August 27th-28th, 2015 (see sections 3.2, 4.5)
IRMS_EA	Peat core (collected at Field Site location, see Figure 1b) data produced from isotope ratio mass spectrometer and elemental analyzer analysis (see sections 3.2, 4.5)